National Technical University of Athens
School of Mechanical Engineering
Department of Fluid Mechanics
Laboratory of Aerodynamics

SIMULATION OF THE FLOW FIELD AROUND BUILDINGS USING A FREE-WAKE VORTEX METHOD

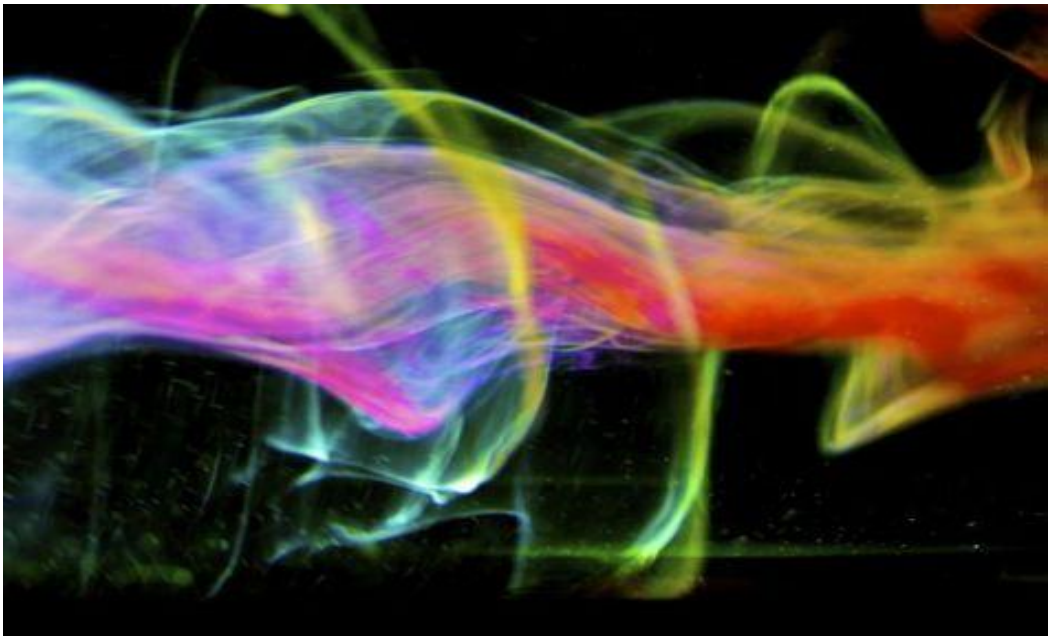

Diploma Thesis

Ioanna-Christina Paparizou

Supervisor: Vasilios Riziotis, Assistant Professor

Athens, March 2019

Acknowledgments

First of all, I would like to express my sincere gratitude to my professor Vasilios Riziotis who supported me through the procedure of writing my thesis. His continuous guidelines along with his willingness to solve and discuss my queries about the subject led me to approach my thesis with creative thought and enthusiasm. I would like also to thank Theologos Andronikos for guiding me in the initial crucial steps of the research. In general, my experience of working my thesis in the Aerodynamics Lab of is very positive, since the mentality of the personnel encourages the creative and authentic productivity. My friends, family and second family never stopped believing in me and stood by my side even in the most challenging times. This strong support system played a catalyst role in the completion of my thesis.

The image of the cover page is a sample of Pery Burge's work. Her amazing art is focused on flow visualization. One can deeply comprehend the laws of nature, through the path of art. Rest in peace Pery and thank you for your huge contribution in the Art-Science community…

To my father Leonidas Paparizos

Dadi, mi-e dor de tine

Abstract

Complex problems, such as the rotor flight in the vicinity of a building, demand an increased computation time when solved with the URANS method. The aim of this thesis is to construct a formulation based on the panel method (potential flow combined with a free-vortex model for the flow separation from the edges of the body) for the simple case of a building embedded in a free-stream flow. The desired outcome is a valid calculation of the pressure distribution along the building and not the generation of the exact flow field, since the viscous terms and turbulence prediction are neglected in this time-efficient approach.

At first, the basic characteristics of wind-building interaction are briefly analysed in order to comprehend the differences between streamlined - bluff body aerodynamics (panel methods are widely applied in lifting surfaces). The challenge of this bluff geometry is the simulation of the flow separation with a free-vortex model. For the solution of the problem the direct formulation (Morino & Kuo) is applied and two alternative implementations of the Kutta condition are examined for the calculation of the circulation shed on the near wake combined with the imposition of the no-penetration condition at the collocation points of the body (constant potential distributions along each panel). The results are compared with experimental data and CFD simulations of the same model. For a valid calculation of the Cp the inviscid method constructed in this thesis can be applied at the complex rotor - bluff obstacle problem, in order to examine their aerodynamic interaction and obtain the induced loads in both bodies.

Contents

1. Introduction

Computational Fluid Dynamics (CFD)

The fundamentals of fluid mechanics constitute the starting point to designing a solution for an engineering flow problem. In order to model the real problem, assumptions for the flow need to be made. The equations that govern the problem cannot be solved analytically, thus numerical formulations are structured suitably. The quality of a CFD model lies in the intersection of its effectiveness and efficiency. Depending on the nature of the problem, different methods are applied and in some cases hybrid models based on the coupling of these methods are developed.

The basic laws that govern the fluid motion in general are the conservation of mass, momentum and energy. For low speed aerodynamics problems, in which the Mach number is within the range 0-0.3, the flow can be assumed as incompressible. A fluid is characterised as compressible when its density is altered significantly with the variation of pressure. Another basic property of the fluid is its viscosity, which is defined as the measure of its resistance to gradual deformation by shear stress. In simple terms, viscosity is translated as friction between the elements of the fluid. The Navier - Stokes equations in the differential form describe the motion of fluids and correspond to the conservation of momentum.

$$\rho \frac{D\mathbf{U}}{Dt} = -\nabla p + \mu \nabla^2 \mathbf{U} + \rho \mathbf{g} \tag{1.1}$$

In continuum mechanics, the vorticity is a pseudovector field that describes the local spinning motion of a continuum near some point (the tendency of something to rotate), as would be seen by an observer located at that point and travelling along with the flow. As presented in 1.2 the shear stresses are interrelated with the vorticity field. Friction forces do not only occur due to the viscosity internal property of the fluid, but also due to a macroscopic development of vorticity (in the region outside the boundary layer).

$$\boldsymbol{\omega} = \nabla \times \mathbf{U} \tag{1.2}$$

CFD is a branch of fluid mechanics that uses numerical analysis and data structures in order to solve the equations that govern the flow fields. Aerodynamics has been a catalyst to there rapid development of this research field. The capacity of CFD is defined by the available computing power and the numerical behavior of the algorithms used for the solution of the equations. The set of Navier - Stokes equations is the most commonly used mathematical model in CFD. The geometry of the body to be analyzed is essential for extracting the fluid domain. The mesh is designed by the discretization of this domain into cells that can be a combination of hexahedral, tetrahedral, prismatic, pyramid or polyhedral elements. The mesh can be uniform or non-uniform, structured or unstructured depending on the problem

and its dimensions extend approximately 10D from the body in all directions, where D is the characteristic length of the body.

In such methods, where the mesh is fixed, the Eulerian specification of the flow field is applied. For an unsteady and incompressible flow, at each timestep the unknown variables u,v,w and p are calculated on the nodes of the mesh. This calculation is a result of the iterative numerical solution of the Navier - Stokes equations in combination with boundary and initial conditions. The most common numerical methods that fall into this category are FVM, FEM and FD. The disadvantage of these methods is the number of degrees of freedom which leads to a significant increase in computation time. Using finer grid resolution in areas of low velocity and pressure gradients is a way of reducing the number of degrees of freedom. Parallel computing, by using simultaneously more than one processor for the execution of the program, has reduced significantly the computation time of complex problems.

The non-linear convective term of 1.1 introduces a complexity in the numerical solution of the equations, since computers are efficient in solving matrices. The linearization of equations with respect to the physics of the problem is necessary in order to reduce the computational cost. Another category of methods which are based on the Lagrangian specification of the flow field are the inviscid panel methods that will be presented in the next chapter. The main advantage of these methods, is the computation time efficiency due to the linear nature of the governing Laplace equation and the significantly reduced number of degrees of freedom. The assumption of inviscid flow is made in cases where the friction forces acting on the fluid particles are negligible compared to the inertial ones. In cases of streamlined bodies, the inviscid flow assumption leads to a sufficient approximation of the real flow and therefore is widely used. Conversely, in aerodynamic problems where intensive turbulent phenomena occur, such as flow separation and the atmospheric boundary layer, this assumption does not lead to a valid solution but only to an approximate one.

Turbulence Models

Almost every real flow is turbulent, with occurring fluctuations around the mean value of velocity in the micro scale of time, so for a valid solution to be obtained the RANS (Reynold Averaged Navier Stokes) equations coupled with a turbulence model need to be solved. Turbulence models are simplified constitutive equations that predict the statistical evolution of turbulent flows. But even the latter method is considered to be reliable only for attached flows. For smooth-body separation bubbles in particular, most RANS models are known to under predict the turbulence levels within the separated shear layer. As a result, reattachment and subsequent boundary layer recovery is typically delayed.

Especially for atmospheric flows, for an accurate solution to be obtained, the effect of turbulence cannot be neglected. The field of bluff body aerodynamics is constantly growing and research is focused on the modelling of turbulence. Experimental data is widely used in these cases for the validation of the developing methods. In many cases of engineering problems, the existing methods are being alternated and appropriate formulations are structured depending on the problem and on its aim of research. Particularly, in the case examined in this thesis, an approximated formulation is designed and flow turbulence is not modelled. The purpose of the research is to obtain the pattern of the separated flow around the building and use it for other aerodynamic problems as the undisturbed flow field. One case of interest is the flight of a helicopter near a building structure.

Bluff Body Aerodynamics

The aerodynamic simulation of buildings, except from the calculation of loads for structural analysis (pressure distribution, vortex shedding), is essential for other cases such as ventilation, air pollutant concentration in cities, pedestrian comfort etc. The understanding of the basic characteristics of the wind-building interaction is necessary for constructing the inviscid computational tool which is the subject of this thesis.

The geometry of the building (bluff) is the reason it behaves in a different manner than an airfoil (streamlined) when exposed to a stream of air. A bluff body is defined as a body that, as a result of its geometry, has separated flow over a substantial part of its surface and consequently an increased drag force.

Reynolds number is defined as:

$$\mathrm{Re} = \frac{U_\infty D}{v} \qquad 1.3$$

In the expression above U_∞ represents the freestream velocity, v the kinematic viscosity of the fluid and D the characteristic length of the body. In the case of the building examined the lateral dimension (x direction) is considered as the characteristic one.

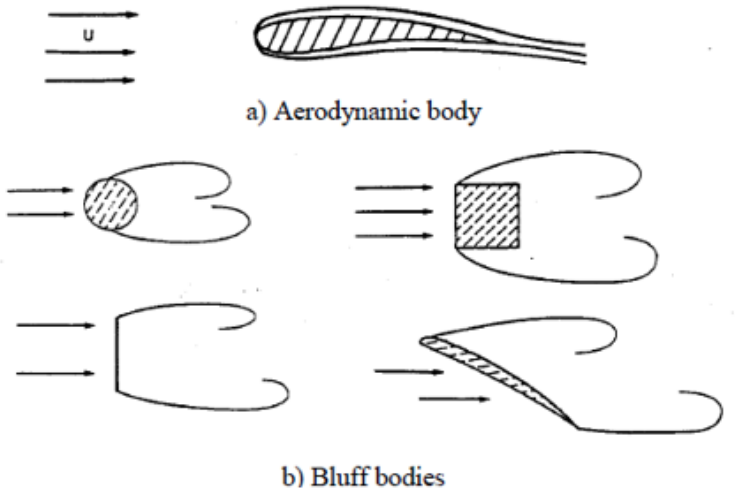

Figure 1.1: Extended wake due to flow separation occurs in bluff bodies

Flow separation

Flow separation is a viscous phenomenon and refers to the detachment of the flow from the solid boundary due to an adverse pressure gradient. The boundary layer thickens at the separation point and the flow is reversed leading to the formation of vortices and eddies, consequently the division of the flow field at an inviscid and viscid (recirculation) region Figure 1.2.

In non-symmetrical bodies as the airfoil presented in Figure 1.1 , the different velocities that occur on the upper and lower side for the same x position correspond to the occurrence of circulation around the body ($\Gamma_B \neq 0$) and consequently a thin wake (shear surface with concentrated vorticity) is emitted from the trailing edge of the body. Conversely, in symmetrical bodies embedded in a zero-incidence flow, such as the sharp-edged prism examined in this thesis, the flow field is symmetric and thus the potential flow solution leads to a zero drag force. This potential approach opposed the experimental measurements on bluff bodies, that denoted the presence of a high drag force acting on the body (D' Alembert Paradox).

The inability of the fluid particles to turn around the sharp edge leads to the emission of a wake and is the explanation of the latter paradox. So, even in the inviscid approach, which neglects the boundary layer, the separated flow needs to be modeled with a vortex method. In the case of sharp edges, the separation point position and the emission velocity of the near wake are known Figure 2.9.

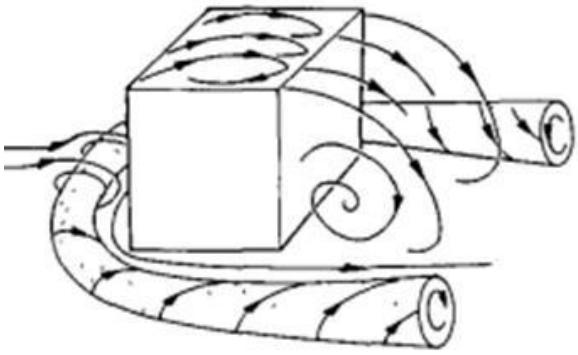

Figure 1.2: Recirculation region and horseshoe vortex (3D)

Vortex shedding

A characteristic of the flow around a bluff body is the Karman vortex street phenomenon, which is defined as a repeating pattern of swirling vortices caused by a process known as vortex shedding. This oscillating flow pattern induces vibration on the body and in the unwanted case of frequency synchronization there is a chance of structural collapse (Tacoma Narrows Bridge, 1940).

The dimensionless Strouhal number characterizes the oscillation of the flow:

$$St = \frac{fD}{U_\infty} \qquad 1.4$$

An important observation is its independence from the viscosity of the fluid.

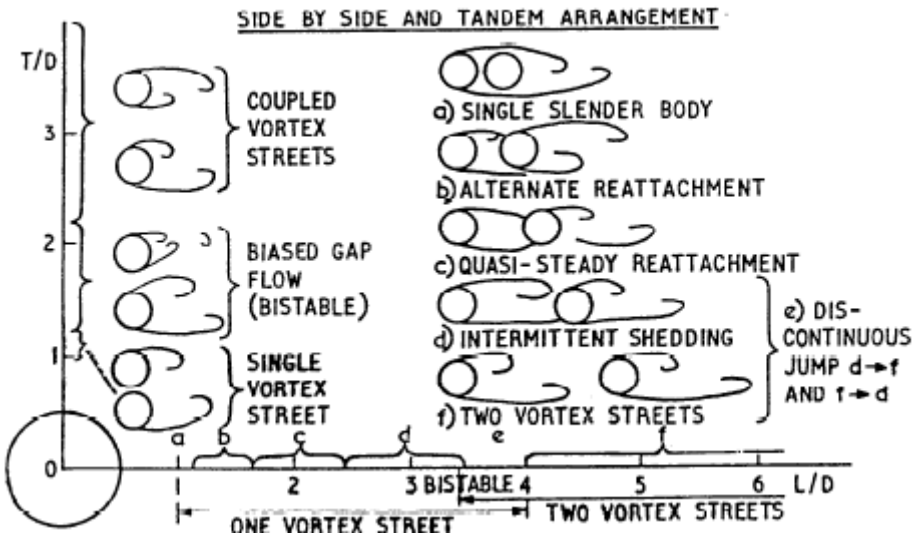

Figure 1.3: Different relative positions of two bluff bodies leads to different Karman vortex street formation *(1)*

The building (single bluff body) corresponds to the case of the two spheres placed in a very small relative distance that lead to the formation of a single vortex street.

For low Reynolds numbers the shedding of the vortices is stable (symmetric) but as the Re increases (around 120 for the case of the building), as stated in (1) "*the steady configuration becomes unstable, starting from the downstream end of the recirculating region, and a new time-dependent equilibrium flow is reached, which is characterized by the regular alternate shedding of vortices, with a definite frequency f, from the two sides of the body*"

Effect of Turbulence

A turbulent flow sustains a smaller wake, since with the intense mixing that takes place between the fluid particles an amount of kinetic energy is transferred to the region near the surface and thus the reversion of the flow at the separation point is delayed.

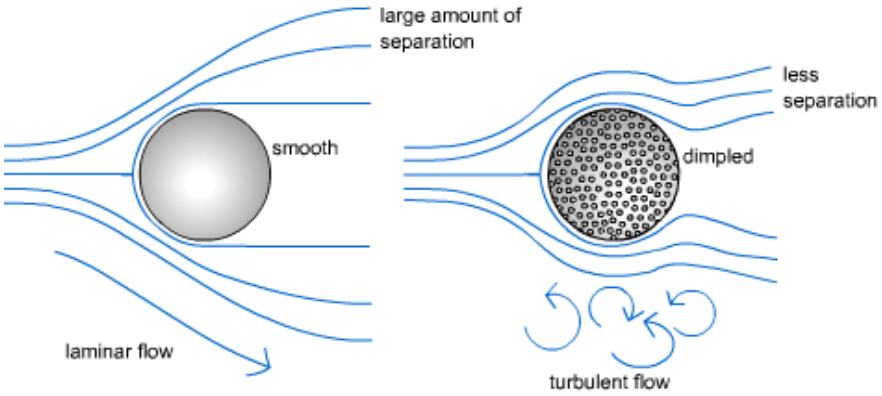

Figure 1.4: The dimples in a golf ball induce turbulence and a reduced drag force

The building, which is the point of interest in this thesis, is modelled by a rectangular prism and in reality, is on the vicinity of the surface layer (10% of Atmospheric Boundary Layer). In this region the turbulence intensity is high and increases as the ground level is approached. The simplicity of the prism geometry contradicts the complex turbulent flow characteristics that govern the problem. Thus, the turbulence prediction models used in the CFD tools need to be verified by comparison with existing experimental data. In the section bellow results from the bibliography will be presented in order to comprehend the basic characteristics of the flow around a building.

The source of Figure 1.5, Figure 1.6 is the publication of (2) and the subject is the strong dependence of the aerodynamic behavior of the bluff geometry on the Reynolds number and the turbulence prediction model. The case of this research is a 2D rectangular shape with an aspect ratio 5:1 and the ABL was not incorporated in the freestream. Thus, the presence of strong turbulent characteristics in the wind-bluff body is independent from the incorporation of the ABL.

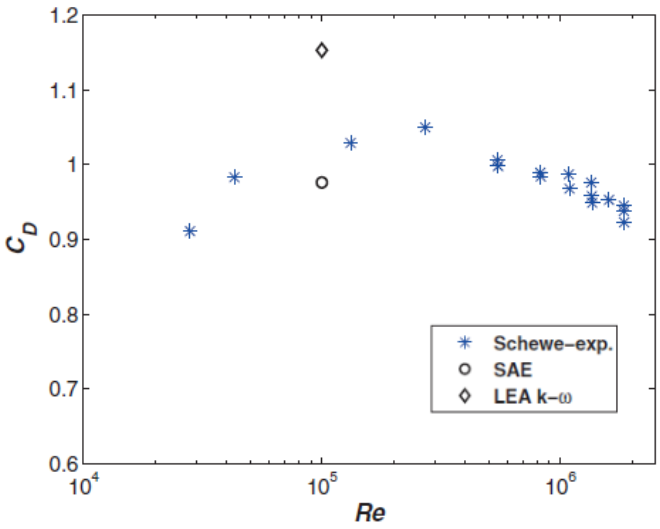

Figure 1.5: As the Re numbers increases (turbulent flow) the drag coefficient is reduced

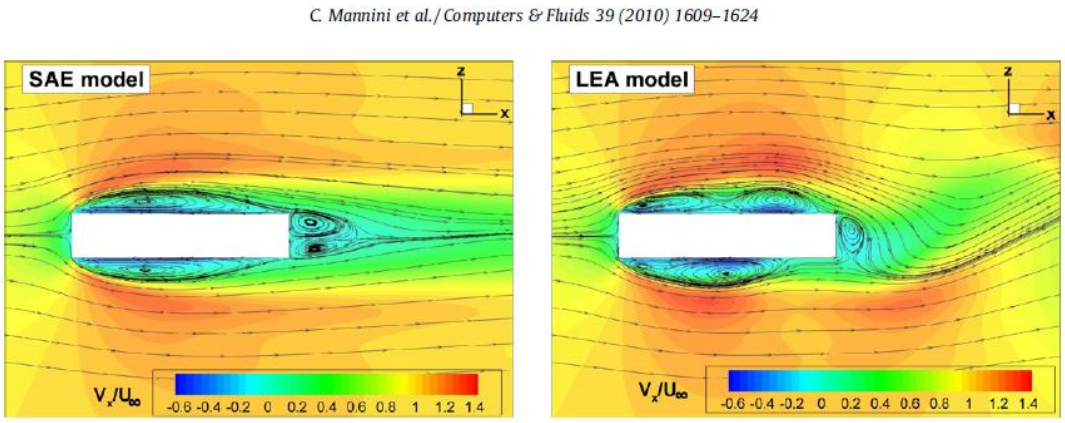

Figure 1.6: SAE model yields an almost steady flow field which contradicts the expected oscillating vortex shedding phenomenon that is generated with the LEA model

As presented in Figure 1.7, the CFD and experimental results yield the same pressure distribution on the rear plane and differ on the top plane due to the prediction model of turbulence as depicted in Figure 1.6.

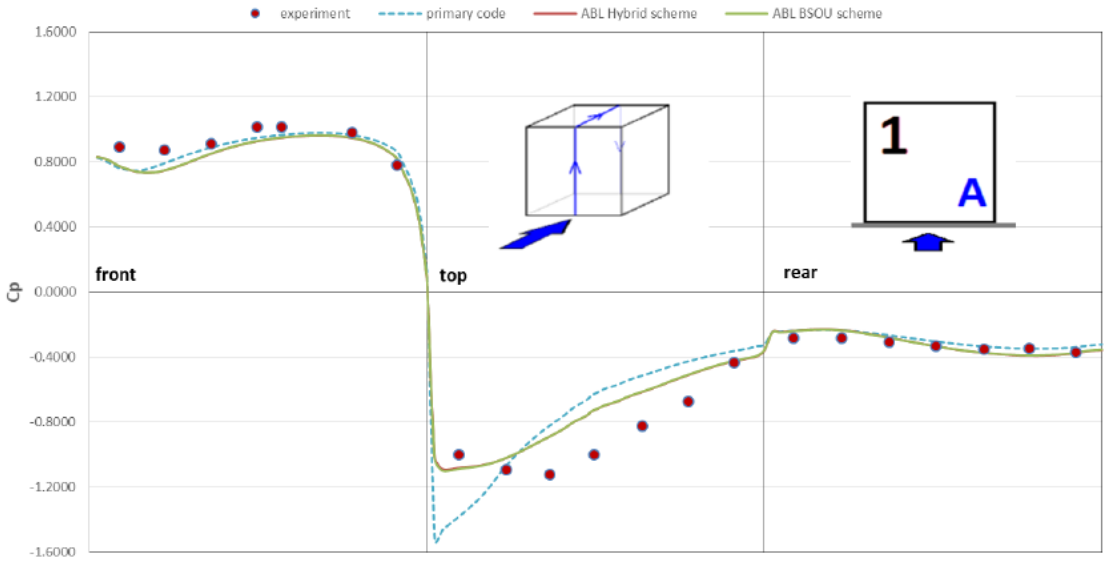

Figure 1.7: The graph is obtained from the diploma thesis of *(3)*

Statement of the Problem

The method applied in this thesis for the simulation of the flow around a building (bluff body of rectangular shape) is the meshless vortex method and thus no turbulence prediction model will be included. The motivation is to obtain the pressure distribution over the body and not the exact flow field. The essential characteristic of bluff body aerodynamics that needs to be modelled with the EIF method for the desired outcome is the separation of the flow from the rear trailing edge S (the separation from the side edges is not modeled). The case of the building examined corresponds to a high Reynolds number flow. As stated above (1) the instability that triggers the vortex shedding phenomenon is located at the downstream end of the recirculation region R Figure 1.8. Therefore, the first step is to achieve the recirculation zone formation with the vortex method and for time efficiency reasons the system of solutions will be considered symmetrical (Symmetrical Solutions). The right amount of vorticity shed on the near wake is the key point of the recirculation zone formation (suction on the rear plane).

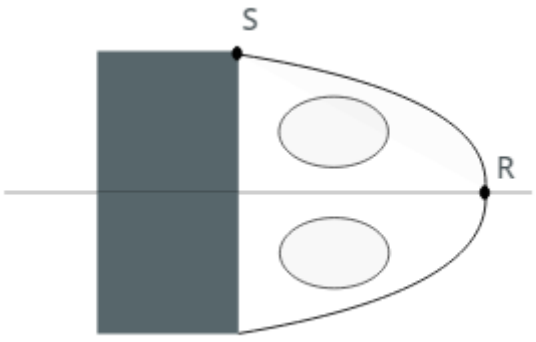

Figure 1.8: Stable formation of symmetric vortices at the first timesteps

Thesis Outline

- Chapter 2: The basic equivalent inviscid flow is presented in terms of the panel method and the free vortex model.
- Chapter 3: Two different formulations based on the implementation of the Kutta condition and the method of solution are presented along with the numerical details of the problem.
- Chapter 4: The results of the formulations are analyzed and compared with CFD (3), (4) and experimental simulations (5).
- Chapter 5: The most important observations of the method and proposals for future investigation are presented.

2. Equivalent Inviscid Flow (EIF)

The efficient panel method, usually characterized as inviscid, takes into account the shear layer of the separation wake in order to approximate real flow. This approach is considered as EIF since although the viscous terms are being neglected, the effects of viscosity that affect the pressure field are combined with the potential flow (wake model, Kutta condition, cut off length parameter etc.).

VORTEX THEORY

The wake region, which in the particular problem simulates the separation of the flow, cannot be neglected and in order to construct a suitable model the basic vortex theory in EIF needs to be examined.

Circulation is defined as the line integral around a closed curve C of the velocity field.

$$\Gamma = \oint \mathbf{U} \cdot \mathbf{dl} \tag{2.1}$$

Kelvin's Circulation Theorem

According to this theorem the circulation Γ is materially conserved. The closed curve C is considered to lay on the surface of the body spanwise.

$$\frac{D\Gamma}{DT} = 0 \tag{2.2}$$

At t=0 the circulation around the body Γ_B is zero. As the flow develops this value increases and consequently with respect to Kelvin's Theorem a vortex of equal strength Γ_B and opposite sign needs to be emitted from the body, known as the starting vortex. Thus, by analysing the material derivative the vorticity shed on the near wake at every timestep is connected with the time rate of change of circulation around the body.

$$\frac{\partial\Gamma}{\partial t} = -\frac{\mathbf{dl_w}}{dt}\boldsymbol{\gamma_w} \tag{2.3}$$

Helmholtz's Theorems

The theorems presented below, describe the three-dimensional motion of fluid in the vicinity of vortex filaments. These theorems apply to inviscid flows. In observations of vortices in real fluids the strengths of the vortices always decay gradually due to the dissipative effect of viscous forces.

1) The strength of a vortex tube does not vary with time.

2) Fluid elements lying on a vortex line at some instant continue to lie on that vortex line. More simply, vortex lines move with the fluid. Also, vortex lines and tubes must appear as a closed loop, extend to infinity or start/end at solid boundaries.

3) Fluid elements initially free of vorticity remain free of vorticity.

For the understanding of these theorems a brief description of vortex lines, vortex tubes and vortex filaments needs to be made. The field lines that are parallel to the vorticity vector are called vortex lines. The vortex lines passing through a closed curve in space form a vortex tube. A vortex filament is defined as a vortex tube of infinitesimal cross-sectional area, which leads to an infinite value for the vorticity. To overcome this singularity and for the purpose of modeling it is convenient to define a vortex filament with a fixed circulation, zero cross-sectional area, and infinite vorticity as a vortex filament with concentrated vorticity. The strength of this element it is the fixed circulation specified through Stokes's Theorem 2.4.

$$\Gamma = \oint \mathbf{U} \cdot \mathbf{dl} = \int_S \boldsymbol{\omega} \cdot \mathbf{n}\, dS \qquad 2.4$$

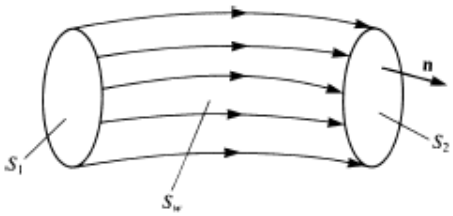

Figure 2.1: Vortex tube *(6)*

The Green's divergence theorem states that the divergence of the curl of any vector is identically zero. An application of the divergence theorem leads to

$$\int_S \boldsymbol{\omega} \cdot \mathbf{n}\, dS = \int_V \nabla \cdot \boldsymbol{\omega}\, dV = 0 \qquad 2.5$$

In the equation above, R is considered the space enclosed in the surface S of the vortex tube and vorticity q is defined as the curl of velocity. This yields to

$$\int_S \boldsymbol{\omega} \cdot \mathbf{n}\, dS = \int_{S_1} \boldsymbol{\omega} \cdot \mathbf{n}\, dS + \int_{S_2} \boldsymbol{\omega} \cdot \mathbf{n}\, dS = 0 \qquad 2.6$$

The vector **n** is the outward normal with its direction shown in Figure 2.1. By defining $\mathbf{n_u}$ the normal vector being positive in the direction of the vorticity 2.5 leads to

$$\int_{S_1} \boldsymbol{\omega} \cdot \mathbf{n_U}\, dS = \int_{S_2} \boldsymbol{\omega} \cdot \mathbf{n_U}\, dS = \text{const} \qquad 2.7$$

The equation above is translated to the quantity of 2.6 being the same for any cross-sectional surface of the tube at any timestep. A consequence of this proof is that Kelvin's and Helmholtz's theorems are equivalent.

Biot-Savart law

With its roots in electromagnetism, this law is broadly used in inviscid aerodynamics problems in order to calculate the induced velocity field from a vorticity distribution. In the general case, the induced velocity in an arbitrary point P from a vortex segment of strength Γ, where **r** is the distance from the influencing point to point C and **dl** the length of the element, is given by the following expression.

$$\mathbf{u_{ind}} = \frac{\Gamma}{4\pi} \frac{\mathbf{dl} \times \mathbf{r}}{|\mathbf{r}|^3} \qquad 2.8$$

Especially, when the vortex segment is a vortex filament, which is part of a closed vortex line the induced velocity is written

$$\mathbf{u_{ind}} = \frac{\Gamma}{4\pi} \frac{(r_1 + r_2)\,(\mathbf{r_1} \times \mathbf{r_2})}{(r_1 r_2)(r_1 r_2 + \mathbf{r_1} \cdot \mathbf{r_2})} \qquad 2.9$$

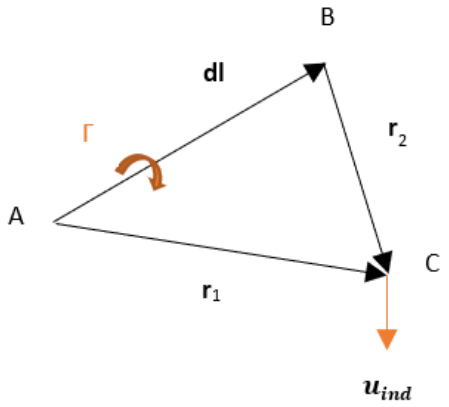

Figure 2.2: The Biot-Savart law for a vortex filament *(7)*

Vortex Lattice Method (VLM)

In this dynamic method the wake is modeled as a free lattice consisting of interconnected concentrated vorticity elements known as vortex rings Figure 2.3. These singularities are represented by panels whose sides are vortex filaments forming a closed curve accordingly to Helmholtz's second theorem. The segment of each element is defined by two points known as the Lagrangian markers and because the vorticity is a vector, let (A) be the head and (B) the tail of the segment Figure 2.2. The vortex lattice is characterized as free, due to the movement of the wake, which is based on the calculation of the induced velocity (Biot-Savart law) at each node of the surface. This independent computation of the velocity at the markers of each panel may lead, in case of numerical instabilities, in the unwanted deformation of the element and consequently the lattice. By applying Kelvin's theorem on the body-near wake material system, the constant strength Γ_{wi} of each near wake panel is obtained and conserved over time (Helmholtz's first theorem) and convicted to the far wake based on the procedure described above.

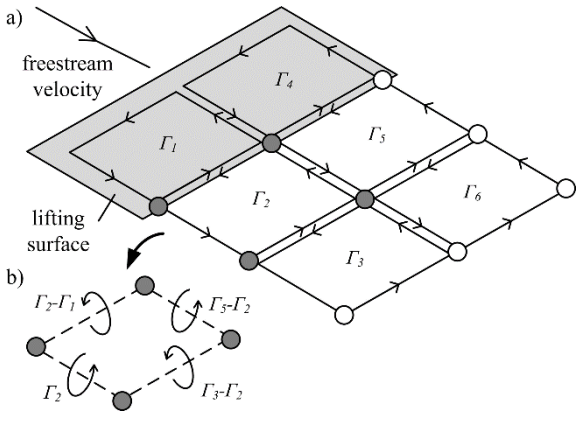

Figure 2.3: Vortex rings structuring the vortex lattice

Vortex Particle Method (VPM)

The particle method for modelling the occurring vorticity in inviscid flows, is based on representing the wake region with discrete elements (particles) instead of a continuous surface (vortex lattice). The particles are modeled as point vortices; thus, the induced velocity is calculated by the Biot-Savart law.

$$\boldsymbol{u}_{\omega}(\boldsymbol{x}) = \frac{1}{4\pi} \sum_{p} \frac{\boldsymbol{\omega}_P \times (\boldsymbol{x} - \boldsymbol{x}_P)}{|\boldsymbol{x} - \boldsymbol{x}_P|^3} \qquad 2.10$$

The tendency of a fluid particle to spin is described by the local strength of vorticity ω. The near wake is modelled as a vortex sheet and the vortex rings of the far wake region are replaced by vortex particles, by concentrating the distributed vorticity to the material points. Hence, it is possible to replace a set of vortex rings that cover a surface D of the wake region with a single particle P 2.11 and achieve the reduction of the vortex element. The VPM is applied in cases where the VLM leads to numerical instabilities, such as the roll up region of the wake.

$$\boldsymbol{\omega}_P = \int_D \boldsymbol{\gamma}(\boldsymbol{x}, t)\, dD \qquad 2.11$$

PANEL METHOD

The Panel Method (PM) is the Boundary Elements Method (BEM) applied to fluid dynamics. Especially in the field of aerodynamics, panel methods have been sufficiently developed for routinely analysing even complex geometries. The core idea of this method is the distribution of singularity elements on small quadrilateral portions, called panels, on the surface of the body. The flow is generated by the superimposition of source, doublet and vorticity singularity elements depending on the physics of each problem. The panel method is applied in cases of the inviscid flow assumption under the assumption of the inviscid flow. Consequently, important viscous flow behaviour such as separation cannot be predicted by this method. The objective of this thesis, is to design a panel method formulation that simulates the separation of the flow over the building and results to an approximated solution, based on the assumption that separated flow regions can be represented by thin vortex shear layers (8), (9), (10).

Helmholtz decomposition

This theorem is known as the fundamental theorem of vector calculus and it states that any vector field that is finite, continuous and continuously differentiable, can be resolved into the sum of an irrotational (curl-free) vector field and a solenoidal (divergence-free) vector field. In fluid mechanics the application of this theorem yields to the following expression for the velocity field.

$$\mathbf{U}(\mathbf{x},\mathrm{t}) = \mathbf{U}_{\infty}(\mathbf{x},\mathrm{t}) + \nabla\Phi(\mathbf{x},\mathrm{t}) + \nabla \times \mathbf{A} \qquad 2.12$$

The irrotational velocity field derives from the divergence of the velocity potential and the term $\nabla \times \mathbf{A}$ represents the induced velocity from the wake at a point **x** on the flow field D.

Potential flow

A potential flow is an ideal flow characterized as inviscid, irrotational and linear. The condition that describes an irrotational flow field is $\boldsymbol{\omega} = 0$ for every fluid element of the field. In such cases the disturbed velocity field can be obtained by the dot product of the potential scalar field 2.10. For an incompressible and irrotational flow the continuity equation transforms to the Laplace linear equation 2.11 .

$$\mathbf{u} = \nabla\Phi \qquad 2.13$$

$$\nabla^2\Phi = 0 \qquad 2.14$$

Singularity Elements

The linear nature of Laplace equation allows the superimposition of basic solutions which in the method analysed are the boundary element singularities. In many cases it is preferable to distribute doublet elements which are scalar rather than vortex because surface vorticity is a vector. Elliptic equations, such as the Laplace equation, have the property that the presence of a basic solution at an influencing point Q($\mathbf{x}_Q$) is felt as a disturbance at any arbitrary point P($\mathbf{x}_P$) of the flow field, although the effect usually dies out rapidly with distance, as presented in 2.15, 2.16.

The basic solutions which satisfy the Laplace equation are called unit point source and doublet and their expressions are presented below:

Point source:

$$\Phi_p{}^{\sigma}(\mathbf{x}_Q) = -\frac{1}{R} \tag{2.15}$$

Point doublet:

$$\Phi_p{}^{\mu}(\mathbf{x}_Q) = \mathbf{n}\,\nabla_Q \frac{1}{R(\mathbf{x_P}\,,\,\mathbf{x_Q})} = \mathbf{n}\,\frac{-\mathbf{R}(\mathbf{x_P}\,,\,\mathbf{x_Q})}{R^3} \tag{2.16}$$

Where R is the distance between the influenced point P and the influencing point Q and is given by

$$R = \sqrt{(x_Q - x_P)^2 + (y_Q - y_P)^2 + (z_Q - z_P)^2} \tag{2.17}$$

A more general approach based on the superimposition of the basic solutions, which is used to model aerodynamic problems, is Green's third theorem:

$$\Phi_p = \int_S \left[\sigma K_\sigma + \mu K_\mu\right] dS_Q \tag{2.18}$$

In the expression of the velocity potential presented above, σ, μ stand for the strengths of the point source and doublet unknown distributions accordingly and Kσ, Kμ for the aerodynamic influence coefficients (AIC) of the elements. The surface S represents a surface of discontinuity, which is discretized in panels of surface dS_Q. For cases of incompressible flow, the panels that model the surface are usually flat. The strengths σ and μ of the source and doublet elements respectively are known as density functions and are equal to jumps (discontinuities) 2.19 , 2.20 across the panels and are the unknown values of the problem. As presented in Figure 2.4 the solid boundary S_B divides the problem in an external and an internal. In the following equations the strengths μ, σ of the boundary elements are presented.

$$\mu = -[[\Phi]] = -(\Phi^+ - \Phi^-) \tag{2.19}$$

$$\sigma = \left[\left[\frac{\partial \Phi}{\partial \mathbf{n}}\right]\right] = \frac{\partial \Phi^+}{\partial \mathbf{n}} - \frac{\partial \Phi^-}{\partial \mathbf{n}} \tag{2.20}$$

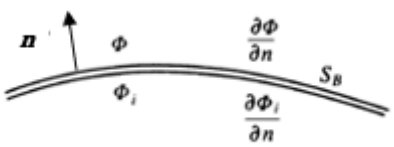

Figure 2.4: The discontinuity surface S_B *(6)*

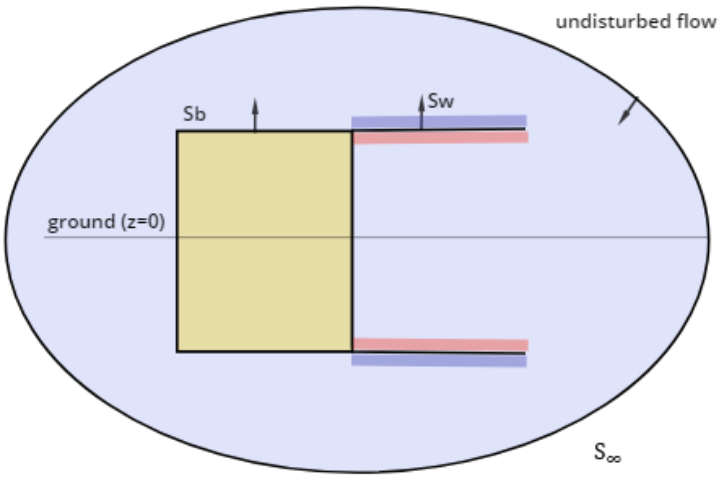

Figure 2.5: The elements that generate the disturbed flow field are distributed along the discontinuity surfaces S_B, S_w

A functional form is assumed for σ and μ over each panel and boundary conditions are imposed at the control point P of each panel depending on the nature of the problem. For subsonic flows, as the one examined in this thesis, constant source and doublet distributions are chosen for each panel, which is a low-order approach.

Wake Model

The wake can be defined as the flow region of vorticity downstream a body which consists of the fluid particles that have been emitted from the edges of the body since the start of the flow development. Conversely to the classic CFD methods presented previously where the wake generation is a result of the solution, in panel methods (inviscid methods) a wake model needs to be coupled with the potential flow in order to simulate the real problem. The wake is modeled as a shear stress surface, since a discontinuity of the tangential velocity occurs and it is characterized as a vortex sheet. Therefore, the design of the wake model is a core step for the construction of a valid panel method formulation. In unsteady panel methods, where the Lagrangian field specification is applied, the major factor that leads to the increase of the computational time is the generation of the wake in every timestep. In cases of aerodynamic problems where the wake pattern is known, such as the flow over a wing or a blade, a prescribed wake representation can be used in order to solve a steady-state problem which reduces significantly the computational time. For cases of a thin wake, panel methods give valid results. On the contrary, for bluff body aerodynamic problems, the viscous effect of the flow separation cannot be modelled sufficiently as a vortex sheet. As stated before, the aim of this thesis is to obtain an approximated solution for the real problem, so the results of the numerical method are expected to deviate from the experimental.

The first step in constructing a model of a physical problem is to understand the fundamental laws that describe its nature. The VORTEX THEORY and the available methods to

model a surface of concentrated vorticity in EIF Vortex Particle Method (VPM) have been analysed previously. In this section the modelling of the wake with singularity elements and the coupling of the potential flow with the wake will be presented. The Kutta condition corresponds to the incorporation of the viscosity effects on the trailing edge in EIF and is essential for the unique solution of the problem.

Kutta Condition

In general, the trailing edge is defined as the finite corner of the body from which the wake is emitted. For an incompressible flow, no normal stresses are acted on the wake surface, hence at the trailing edge of the body the following condition is applied.

$$P^{+} = P^{-} \leftrightarrow \|P\|_{TE} \qquad 2.21$$

In the case of inviscid flow around a sharp corner, the velocity tends to infinity. The Kutta condition is a mathematical formulation which allows to incorporate the significant effect of viscosity in the inviscid method and smoothens the abrupt change of velocity which opposes the real flow behavior at that point. For the above statement to be valid the vorticity at the trailing edge TE needs to be zero.

$$\boldsymbol{\gamma}_{TE} = 0 \qquad 2.22$$

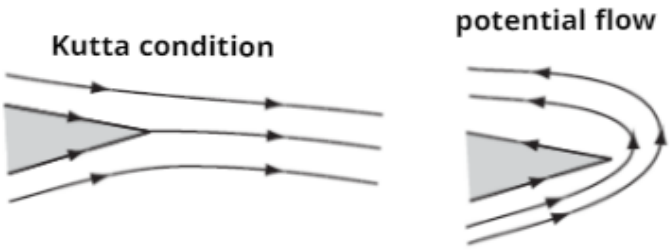

Figure 2.6: Unrealistic acceleration at the TE in potential flow

Based on the basic solution of a point vortex, the equivalence presented below emerges, with the strength of the vortex element $\Gamma_{nw} = -\mu_{nw} = \|\Phi\|_{TE}$. In the 3D case examined in this thesis, the vortex rings can be replaced by a constant-strength doublet distribution along both directions of the panel.

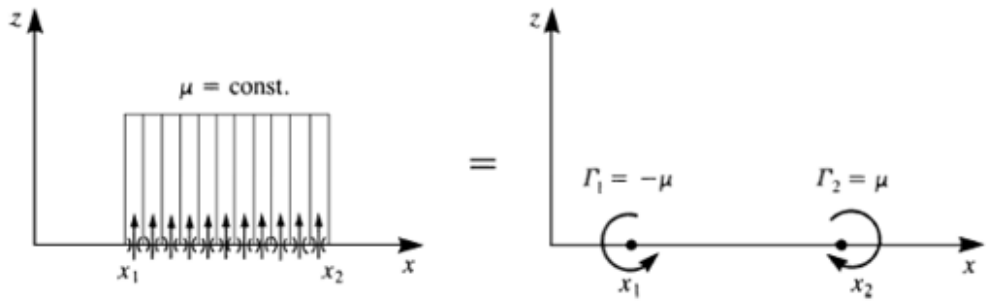

Figure 2.7: Equivalence between a constant-strength doublet panel and two-point vortices at the edge of the panel *(6)*

The wake region has an effect on the whole flow field, including the region over the body. The equivalence presented in Figure 2.7 makes possible the incorporation of the vortex field (wake) in the potential expression 2.18. This coupling in the VLM method is achieved by distributing doublet elements on the wake surface, with the vortex rings being replaced by doublets of constant strength μ_w over the panel. For the case of incompressible flow, the wake source distribution is set to zero and the final mathematical expression of the potential on the body surface based on Green's identity becomes (for **n** pointing on the outward direction from the body). As it has been stated previously according to Kelvin's Theorem the circulation strength $\Gamma_w = \|\Phi\|_w$ of each vortex ring is preserved with time. Therefore, the values of the doublets along the far wake region are known

$$\Phi(\mathbf{x}) = -\frac{1}{4\pi}\int_{S_B}\mu(\mathbf{s})\frac{(\mathbf{x}-\mathbf{s})\cdot\mathbf{n}(\mathbf{s})}{|\mathbf{x}-\mathbf{s}|^3}\,dS - \frac{1}{4\pi}\int_{S_B}\sigma(\mathbf{s})\frac{1}{|\mathbf{x}-\mathbf{s}|}\,dS + \frac{1}{4\pi}\int_{S_w}\|\Phi\|_w(\mathbf{s})\frac{(\mathbf{x}-\mathbf{s})\cdot\mathbf{n}(\mathbf{s})}{|\mathbf{x}-\mathbf{s}|^3}\,dS_w \quad 2.23$$

Alternative Formulations

The core step of engineering design is to construct mathematical formulations that respect the physics and the requirements of each problem. Taking this fact into consideration, alternative formulations can be structured depending on the characteristics of the flow problem. The solution of the particular problem consists of a unique combination of sources and doublets and a set of suitable conditions. The potential flow assumption cannot stand alone in most aerodynamic problems, since a region of vorticity known as the wake is generated from the flow of air over the body. The modelling of the wake is of major importance and will be discussed in the next sub chapter.

The condition that imposes the normal component of the velocity at the solid boundary to be zero is valid in every case, since the fluid cannot penetrate the body. The velocity expression on the body is obtained by differentiating the velocity potential analytically or numerically 2.18 .

$$\mathbf{U} \cdot \mathbf{n} = 0 \tag{2.24}$$

In the equation bellow, **U** represents the velocity flow field, $\mathbf{U}_\infty$ the freestream velocity and **u** the disturbance due to the presence of the body in the field

$$\mathbf{U} = \mathbf{U}_\infty + \mathbf{u} \tag{2.25}$$

Direct formulation

In bodies of substantial thickness which produce a wake, such as the building structure examined, neither the source nor the doublet distribution can be neglected. A popular approach (Morino & Kuo 1974) for the boundary conditions imposed is to set the perturbation potential to zero on the interior side of the panels, since the internal problem is of no interest, which leads to the direct formulation. The Dirichlet boundary condition is verified 2.26 and both the distributions of doublets and source elements are maintained on the boundary. The intensities of the boundary elements are presented in the following equations:

$$\mu(\mathbf{x}) = -\|\Phi\|(\mathbf{x}) = -\Phi^+(\mathbf{x}), \ \mathbf{x} \in S_B \tag{2.26}$$

$$\sigma(\mathbf{x}) = = \left\|\frac{\partial \Phi}{\partial \mathbf{n}}\right\|(\mathbf{x}) = \frac{\partial \Phi^+}{\partial \mathbf{n}}(\mathbf{x}), \quad \mathbf{x} \in S_B \tag{2.27}$$

The Neumann boundary condition 2.28 is applied in order to replace the source distribution as presented in 2.29. Thus, the unknown strengths are limited to the doublet distribution which is equal to the potential Φ over each panel. The formulation is called direct since the unknown potential can be obtained directly by 2.18 or in other words there is a direct correlation between the potential and the density functions 2.26 ,2.27.

$$(\mathbf{U}_\infty + \mathbf{u}) \cdot \mathbf{n} = 0 \tag{2.28}$$

$$\sigma = \mathbf{u} \cdot \mathbf{n} = -\mathbf{U}_\infty \cdot \mathbf{n} \tag{2.29}$$

Indirect formulation

<u>Source element formulation (Hess and Smith 1962)</u>

The velocity field induced by a point source consists only of a radial component. The absence of a tangential component corresponds to an irrotational flow, which is produced in cases of symmetrical (non-lifting) bodies that do not cause the separation of the flow.

$$\mu = 0 \ \rightarrow \Phi^+ = \Phi^- \tag{2.30}$$

The Dirichlet boundary condition 2.30 eliminates the unknown strengths of the problem to the source distribution so in combination with 2.28 and applied for every panel of the body the solution is obtained.

Doublet element formulation (Johnson and Rubbert 1975)

In the case of a thin blade where the aerodynamic body is modelled as a lifting surface the source distribution on the body is set to zero:

$$\sigma = 0 \tag{2.31}$$

The doublet distribution on the body corresponds to a vorticity distribution on the surface 2.32, which leads to the occurrence of circulation at the trailing edge of the body 2.33. In the set of equations below $\boldsymbol{\gamma}(\mathbf{x})$ stands for the surface vorticity.

$$\boldsymbol{\gamma}(\mathbf{x}) = \nabla \mu(\mathbf{x}) \times \mathbf{n}(\mathbf{x}) \tag{2.32}$$

$$\Gamma(\mathbf{x}_{\mathrm{TE}}) = -\mu(\mathbf{x}_{\mathrm{TE}}) = \|\Phi\|_{\mathrm{TE}} \tag{2.33}$$

In this case a Neumann boundary condition 2.28 is imposed and the solution is calculated in a similar way with the Hess source formulation presented above, with the doublet strengths being the unknown of the problem.

Separation Conditions

Bernoulli Energy Equation

The Bernoulli equation is applied between the upper and lower side of the trailing edge and stands for the conservation of energy across the line which connects the two application points. When separation of the flow occurs and a recirculation area (bubble) forms attached to the body, the flow is divided in an inviscid and in a viscid area and the distinction surface is the wake. In the latter case, the energy is not conserved across the line and the transition from the inviscid to the recirculation zone requires an additional term at the Bernoulli equation which represents the residual of energy Dh (loss of mechanical energy along the transition from the inviscid to the viscous region) (11). The unsteady form of the equation is presented below.

$$\frac{\partial \varphi_A}{\partial t} + \frac{U_A{}^2}{2} + \frac{P_A}{\rho} = \frac{\partial \varphi_B}{\partial t} + \frac{U_B{}^2}{2} + \frac{P_B}{\rho} + Dh \tag{2.34}$$

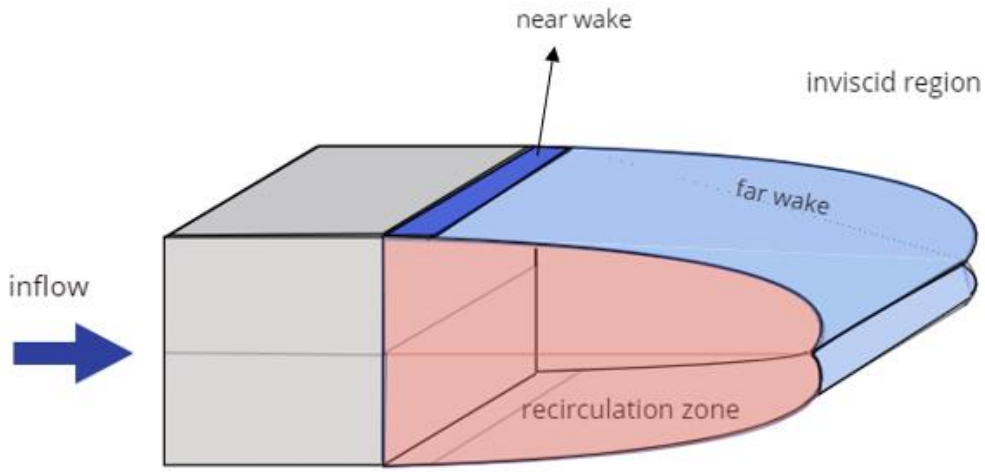

Figure 2.8: Separation of the flow field in two discrete zones, inviscid and recirculation (viscous) region

Stagnation condition

As presented in Figure 2.9 in the case of no separation of the flow at the trailing edge, the **s** local vector is forced to 90 degrees change of direction. This is inconsistent with the physics of the viscid fluid because it would lead to an infinite velocity around the corner. Thus, the **s** component of the velocity is stagnated at the downstream panel (10), (12).

$$\mathbf{U}^{-} \cdot \mathbf{s} = 0 \qquad 2.35$$

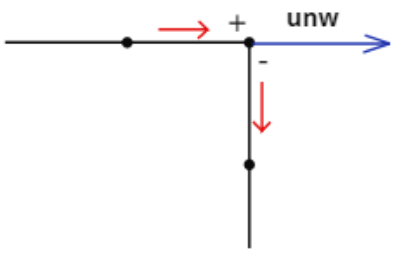

Figure 2.9: Emission of the near wake parallel to the upstream panel

3. Numerical Solution

The theory presented in the previous Chapter is the basis for the analysis that follows, but for a valid solution to be obtained the design of a mathematical model (formulation) custom made for the particular case is essential. This process consists of the discretization of the geometry and equations, the construction of a linear algebraic system and an analysis for the numerical parameters (timestep dt, vortex core radius, etc). The combination of the above steps with an appropriate numerical analysis method yields to the solution of the problem. The fluid flow to be examined is three-dimensional, unsteady, incompressible and assumed inviscid, thus the panel method is applied for the solution.

Ground effect

The ground effect is modelled with the simple mirror-image method by placing a symmetrical about the x axis virtual body. This method is based on the fact that the perpendicular line passing through the midpoint of the segment that connects two symmetrical point vortices is a streamline of the flow field. The imposition of the boundary condition 2.24 on the surface of the ground yields only tangential velocities at the z=0 plane, thus the equivalence presented in Figure 3.1 is proven.

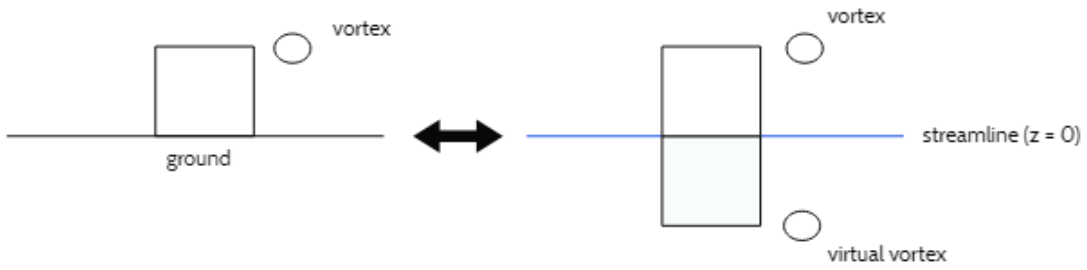

Figure 3.1: Mirror-image ground model

System of equations

As stated previously the crucial step in the simulation of a problem is to design an accurate mathematical model that corresponds to the physics. The model is based on the Direct formulation, the assumption of constant doublet distributions along each panel and the simulation of the flow separation (wake region) with the Vortex Lattice Method (VLM).

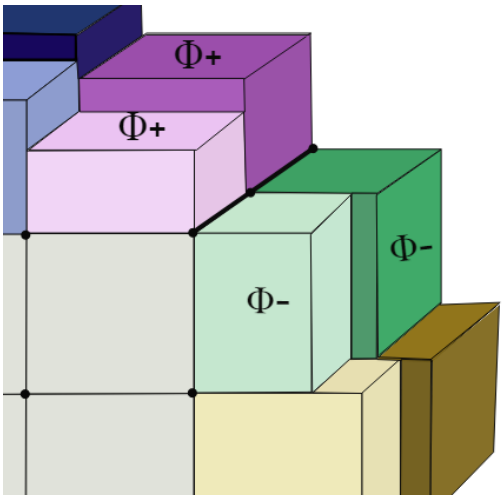

Figure 3.2: Constant distributions along the panels – trailing edge (Illustration)

Green's identity for the potential calculation on a point P $\mathbf{x} \in S_B$ (Direct formulation):

$$\Phi(\mathbf{x}) = \frac{1}{4\pi}\int_{S_B} \Phi(\mathbf{s}) \frac{(\mathbf{x}-\mathbf{s})\cdot\mathbf{n}(\mathbf{s})}{|\mathbf{x}-\mathbf{s}|^3}\, dS - \frac{1}{4\pi}\int_{S_B} (-\mathbf{U}_\infty \cdot \mathbf{n}) \frac{1}{|\mathbf{x}-\mathbf{s}|}\, dS + \frac{1}{4\pi}\int_{S_w} \|\Phi\|_w(\mathbf{s}) \frac{(\mathbf{x}-\mathbf{s})\cdot\mathbf{n}(\mathbf{s})}{|\mathbf{x}-\mathbf{s}|^3}\, dS_w \quad 3.1$$

The far wake region affects the potential $\Phi(\mathbf{x})$ and in order to obtain its desired topology, at the end of every timestep the surface is moved by the calculation of the induced velocity (Biot-Savart law) at each node of the vortex lattice. The circulation of this region is known, since it has been calculated in a previous timestep t_n (Kelvin's Circulation Theorem).

$$\|\Phi\|_{wi,t} = \|\Phi\|_{wi,tn} \quad 3.2$$

t_n corresponds to the timestep when the particular vortex ring was emitted from the trailing edge of the body (near wake).

Consequently, the degrees of freedom at every timestep are limited to the distribution of Φ along the body and $\|\Phi\|_w$ along the near wake panels and the construction of the

algebraic system is held in two alternative formulations (different implementation of Kutta Condition).

The nature of the mathematical model has to coincide with the numerical approach, so the system of equations is structured as a linear system.

$$A\mathbf{x} = B \tag{3.3}$$

The Aerodynamic Influence Coefficients (AIC) are the elements of the square matrix A of N×N dimensions, **x** is the unknown vector of N degrees of freedom and B is the known part of the system and a matrix of N×1 dimension. In order to reduce the DOFs of the system, the assumption of equal solutions for the symmetrical panels of the body and the wake is made. As presented in Figure 3.6 every panel ip has its symmetrical sym(ip) and the new numerical system with N'= N/2 degrees of freedom is a result of superimposing the AIC of the symmetrical panels

$$A'(i,j) = A(i,j) + A\big(i, \mathrm{sym}(j)\big) \qquad , \text{for } i,j = 1, \mathrm{NPANB} \tag{3.4}$$

Formulation 1

This formulation is based on the classic implementation of the Kutta Condition in panel codes that include a thin wake model.

$$\boldsymbol{\gamma}_{TE} = 0 \;\rightarrow\; -\mu_w = -\mu_{T.E} = \|\Phi\|_w = \Phi^+ - \Phi^- \tag{3.5}$$

Thus, the near wake unknown circulation $\|\Phi\|_w$ is defined by the potential distribution on the vicinity of the trailing edge Figure 3.2 and is not considered a degree of freedom for the algebraic system.

The Aerodynamic Influence Coefficients (AIC) of the doublet and source strengths are respectively

$$A_\mu(\mathbf{x},\mathbf{s}) = \frac{1}{4\pi}\frac{r\cdot\mathbf{n}(\mathbf{s})}{|r|^3} \tag{3.6}$$

$$A_\sigma(\mathbf{x},\mathbf{s}) = \frac{1}{4\pi}\frac{1}{|r|} \tag{3.7}$$

In the coefficients presented above **x** represents the coordinates of the control point on the panel of the body (influenced point) , **s** the coordinates of the influencing point (doublet, source surface elements) and $\mathbf{r} = \mathbf{x} - \mathbf{s}$.

The discretized form of the no penetration condition applied at the i =1,..,NPANB collocation points of the body :

$$\Phi(i) = \frac{1}{4\pi}\sum_{j=1}^{NPANB}\Phi(j)*A_{\mu}(i,j) - \frac{1}{4\pi}\sum_{j=1}^{NPANB} -\mathbf{U}_{\infty}(j)\cdot\mathbf{n}(j)*A_{\sigma}(i,j)$$

$$+\frac{1}{4\pi}\sum_{jw=1}^{PAN(nwake)}\left[\Phi(ipanup(jw)) - \Phi(ipandn(jw))\right]*A_{\mu}(i,jw) \qquad 3.8$$

$$+\frac{1}{4\pi}\sum_{jw=1}^{PAN(fwake)}\|\Phi\|_{w}*A_{\mu}(i,jw)$$

The elements of the matrices A'_N , B'_N of the linear algebraic system 3.3:

$$A'_N(i,j) = \begin{cases} -A_{\mu}(i,j) & , \quad j \in [1,i)\cup(i,NPANB) \\ \frac{1}{2} & , \quad j = i \quad \text{singularity} \\ -A_{\mu}(i,j) - A_{\mu}(i,jw) & , \quad j \text{ upstream panel} \\ -A_{\mu}(i,j) + A_{\mu}(i,jw) & , \quad j \text{ downstream panel} \end{cases}$$

$$B'_N(i) = -\frac{1}{4\pi}\sum_{j=1}^{NPANB} -\mathbf{U}_{\infty}(j)\cdot\mathbf{n}(j)A_{\sigma}(i,j) + \frac{1}{4\pi}\sum_{jw=1}^{PAN(fwake)}\|\Phi\|_{w}*A_{\mu}(i,jw)$$

The influence coefficient of the near wake term is embodied in the $A'_N(i,j)$ term of the panels that are upstream and downstream the trailing edge as presented in the figure bellow.

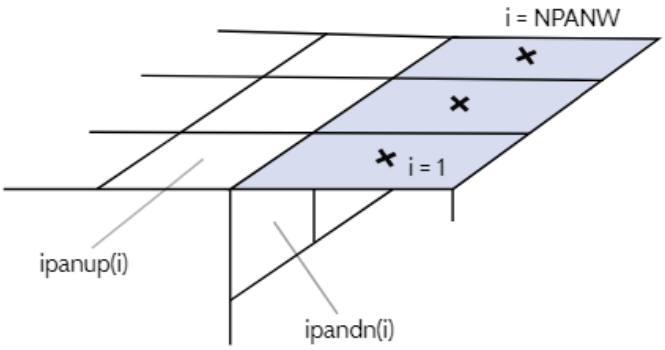

Figure 3.3: interrelation of upstream – downstream panels with the near wake

Formulation 2

The motivation of constructing an alternative formulation is to consider the near wake circulation $\|\Phi\|_w$ as an independent degree of freedom. The pressure implementation of Kutta Condition is used and thus the nonlinear Bernoulli Energy Equation needs to be added to the system. The residual of energy Dh presented in 2.34 cannot be neglected in the case examined in this thesis which is characterized by flow separation.

$$P^+ = P^- \leftrightarrow \|P\|_{TE} \tag{3.9}$$

The unknown distributions of this formulation are the potential Φ along the body, and the $\|\Phi\|_w$ and Dh along the panels of the near wake. Therefore, the auxiliary stagnation condition presented in Separation Conditions is incorporated in order to achieve a well-defined algebraic system.

The equations applied in the formulation need to be linear, in order to compose an efficiently solvable numerical system. The term $\mathbf{U}^{+2}$ in the Bernoulli equation introduces a non-linearity in the system that needs to be handled. The expanded expression of the non-linear term yields

$$\begin{aligned}
&\mathbf{U}^{+2} = \mathbf{U_s}^{+2} + \mathbf{U_t}^{+2} = \left(\mathbf{U_{\infty s}}^{+} + \mathbf{u_s}^{+}\right)^2 + \left(\mathbf{U_{\infty t}}^{+} + \mathbf{u_t}^{+}\right)^2 = \\
&= \left(\mathbf{U_{\infty s}}^{+2} + 2\mathbf{U_{\infty s}}^{+}\mathbf{u_s}^{+} + \mathbf{u_s}^{+\,2}\right) + \left(\mathbf{U_{\infty t}}^{+2} + 2\mathbf{U_{\infty t}}^{+}\mathbf{u_t}^{+} + \mathbf{u_t}^{+\,2}\right) = \\
&= \left(\mathbf{U_{\infty s}}^{+2} + 2\mathbf{U_{\infty s}}^{+}\mathbf{u_s}^{+} + \mathbf{u_{s0}}^{+}\mathbf{u_s}^{+}\right) + \left(\mathbf{U_{\infty t}}^{+2} + 2\mathbf{U_{\infty t}}^{+}\mathbf{u_t}^{+} + \mathbf{u_{t0}}^{+}\mathbf{u_t}^{+}\right) = \\
&= \mathbf{u_s}^{+}\left(2\mathbf{U_{\infty s}}^{+} + \mathbf{u_{s0}}^{+}\right) + \mathbf{u_t}^{+}\left(2\mathbf{U_{\infty t}}^{+} + \mathbf{u_{t0}}^{+}\right) + \left(\mathbf{U_{\infty s}}^{+2} + \mathbf{U_{\infty t}}^{+2}\right)
\end{aligned} \tag{3.10}$$

The expression above is incorporated in the Bernoulli equation and the numerical analysis method chosen for the convergence of the linearized system is the fixed-point iteration:

$$\mathbf{u}^2 = \mathbf{u_0} \cdot \mathbf{u} \qquad 3.11$$

The velocity is initialized $u_0 = 0$ and for the next iterations $\mathbf{u_0}^{i} = \mathbf{u}^{i-1}$.

The convergence criterion is :

$$\mathbf{u_0} = \mathbf{u} \;\leftrightarrow\; \sum_{NDOF} (\mathbf{X}^{i} - \mathbf{X}^{i-1})^2 = 0$$

NDOF represents the number of degrees of freedom **X** and i the convergence iterations in the pseudo-time.

In a similar manner, the non-linear velocity term $\mathbf{U}^{-2}$ of the first spanwise row of panels downstream the trailing edge is analyzed. The velocity needs to be expressed through the unknown strength of the potential in order to construct the desired linear system.

The linearized form 3.10 of the above equation yields the coefficients presented below of the algebraic system. The discretized form of the no penetration condition is presented in Formulation 2.

For $i = NPANB + NPANW, NDOF$ (line of the matrix)

$$A'_B(i,j) = \begin{cases} \left(G^+(i) + G^-(i)\right) * \frac{1}{4\pi} A_{U\mu} & , \quad j \in [1, NPANB] \\ \left(G^+(i) + G^-(i)\right) * \frac{1}{4\pi} A_{U\mu} + \frac{1}{Dt} & , \quad j = ipanup(i) \\ \left(G^+(i) + G^-(i)\right) * \frac{1}{4\pi} A_{U\mu} - \frac{1}{Dt} & , \quad j = ipandn(i) \\ -1 & , \quad j > NPANB + NPANW \end{cases}$$

$$B'_B(i) = D + \frac{\Phi(ip)^{t-Dt} - \Phi(id)^{t-Dt}}{Dt}$$

$$+G^+(i) * \frac{1}{4\pi} \left[\sum_{j=1}^{NPANB} -\mathbf{U}_\infty(j) \cdot \mathbf{n}(j) \frac{\mathbf{r}_{ip,j}}{|\mathbf{r}_{ip,j}|^3} - \sum_{jw=1}^{nfarwake} \|\Phi\|_w(jw) A_{U\mu} \right.$$

$$+G^-(i) * \frac{1}{4\pi} \left[\sum_{j=1}^{NPANB} -\mathbf{U}_\infty(j) \cdot \mathbf{n}(j) \frac{\mathbf{r}_{id,j}}{|\mathbf{r}_{id,j}|^3} - \sum_{jw=1}^{nfarwake} \|\Phi\|_w(jw) A_{U\mu} \right.$$

$\mathrm{ip} = \mathrm{ipanup(i)}$
$\mathrm{id} = \mathrm{ipandn(i)}$
$\mathrm{A_{U\mu}} = \dfrac{\mathbf{dl} \times \mathbf{r}_{\mathrm{ip,jw}}}{\left\lvert \mathbf{r}_{\mathrm{ip,jw}} \right\rvert^3}$
$\mathrm{C_s} = 2\mathrm{U_{\infty s}} + \mathrm{u_{s0}}$
$\mathrm{C_t} = 2\mathrm{U_{\infty t}} + \mathrm{u_{t0}}$
$\mathrm{D(i)} = \frac{1}{2}(-\mathrm{U_{\infty s}}^2(\mathrm{ip}) - \mathrm{U_{\infty t}}^2(\mathrm{ip}) + \mathrm{U_{\infty s}}^2(\mathrm{id}) + \mathrm{U_{\infty t}}^2(\mathrm{id}))$
$\mathrm{G^+(i)} = -\frac{1}{2}\left(\mathbf{s}(\mathrm{ip}) * \mathrm{C_s(ip)} + \mathbf{t}(\mathrm{ip}) * \mathrm{C_t(ip)}\right)$
$\mathrm{G^-(i)} = +\frac{1}{2}\left(\mathbf{s}(\mathrm{id}) * \mathrm{C_s(id)} + \mathbf{t}(\mathrm{id}) * \mathrm{C_t(id)}\right)$
$\mathbf{r}_{\mathrm{l,m}} = \mathbf{x}_\mathrm{l} - \mathbf{x}_\mathrm{m}$, l influenced and m influencing point

Table 3.1

The discretized form of the separation condition yields the coefficients of the algebraic system ($\mathrm{id} = \mathrm{ipandn(ik)}$)

For $\mathrm{i} = \mathrm{NPANB} + 1, \mathrm{NPANB} + 1 + \mathrm{NPANW}$ (line of the matrix)

$$\mathrm{A'_s(i,j)} = \begin{cases} -\mathbf{s}(\mathrm{id}) \cdot \frac{1}{4\pi}\mathrm{A_{U\mu}} & , \ \mathrm{j} \in [1, \mathrm{NPANB}] \\ \mathbf{s}(\mathrm{id}) \cdot \frac{1}{4\pi}\mathrm{A_{U\mu}} & , \ \mathrm{j} \in [\mathrm{NPANB} + 1, \mathrm{NPANB} + 1 \ \mathrm{NPANW}] \\ 0 & , \ \mathrm{j} \in (\mathrm{NPANB} + \mathrm{NPANW}, \mathrm{NDOF}] \end{cases}$$

$$\mathrm{B'_s(i)} = -\mathrm{U_{s\infty}}^-(\mathrm{id}) + \mathbf{s}(\mathrm{id}) \cdot \frac{1}{4\pi}\left(\sum_{\mathrm{j=1}}^{\mathrm{NODESB}} \mathbf{U}_\infty(\mathrm{j}) \cdot \mathbf{n}(\mathrm{j})\left(-\frac{\mathbf{r}_{\mathrm{id,j}}}{\left\lvert \mathbf{r}_{\mathrm{id,j}} \right\rvert^3}\right) + \sum_{\mathrm{jw=1}}^{\mathrm{nfarwake}} \|\Phi\|_\mathrm{w} \mathrm{A_{U\mu}}\right)$$

The two formulations are presented briefly in the table below:

	Formulation 1	**Formulation 2**		
NDOF	NPANB	NPANB + 2*NPANW		
Unknown	Φ_{body}(NPANB)	Φ_{body}(NPANB)	$\|\Phi\|_\mathrm{w}$(NPANW)	Dh(NPANW)

Table 3.2: Methods of solution

Geometry

The specification of the global coordinate system **G** (**x, y, z**) is the first step when inputting the body geometry in the aerodynamic problem.

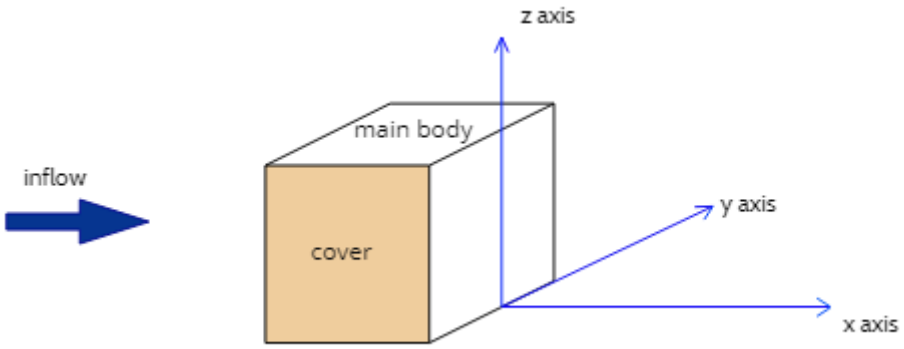

Figure 3.4: Input geometry – global coordinate system

In panel methods, the computational mesh is designed by discretising the body surface in panels. The building structure examined in this thesis is a case of simple geometry assembled by straight surfaces (planes), hence the panels are modelled as quadrilateral rectangular elements. A local coordinate system **L** (**s**, **t**, **n**) lies on each panel. As will be presented below the restriction that needs to be respected is the normal vector **n** to point outward the panel surface. The discretisation of the geometry affects the degrees of freedom of the system.

The geometry of the real body Figure 3.4 is an assembly of the main body and the covers (symmetrical about xz plane). The main body is discretized by placing strips of panels at the spanwise direction, that is considered the y axis and the covers consist of strips of panels at the z direction. Each panel and its local system are defined by the nodes that form it. Thus, the count of the nodes has to be taken in careful consideration when structuring the input

geometry. The computational tool developed in this thesis, generates the virtual body geometry, with respect to the rule mentioned previously for the local system of each panel. The geometry immersed in the flow for the simulation of the problem is presented in Figure 3.5 as an assembly of the different parts described above.

Parameter	Description
NFETES	nodes of main body at the y direction
NODEPF	nodes of main body for a constant y coordinate
NFETEC	nodes of cover for constant x coordinate
NODEPC	nodes of cover for constant z coordinate
NODET	Total nodes of the body
NPANB	Panels of the body

Table 3.3: Basic parameters of input geometry

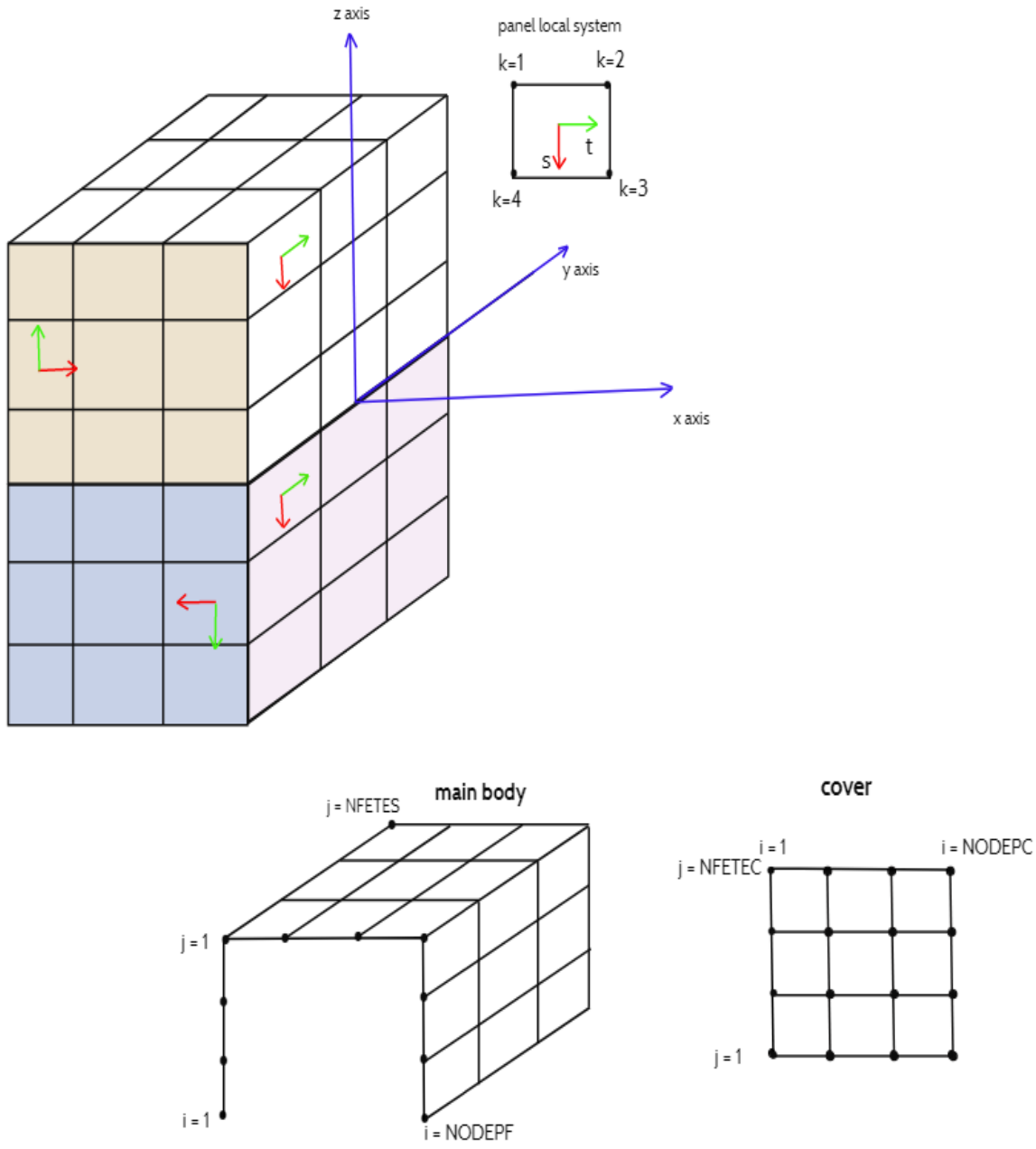

Figure 3.5:Body geometry, local systems at the discrete parts of the assembly, node counters

The normal component **n** of the local system is obtained by the right-hand rule and it is not illustrated in Figure 3.5 for simplicity reasons. The surface is considered parametric S ($\mathbf{s_i}$, $\mathbf{t_j}$) with the incorporation of the local system in the problem.

The global coordinates $\mathbf{X}_G$ (I, n) (I = 1,2,3 three-dimensional global system, n=1,..,NODET) of the real body nodes are imported as input in the code. The next step is to structure the counting of the nodes of the geometry (main body, covers, virtual body) in a way that leads to the desired local systems for each panel. The count (TE) of the local system nodes for each panel derives from the count of the global nodes (n) that form the panel

$$TE(k, ip) = n, \quad k = 1,..,4, \quad ip = 1,2,..,NPAN, \quad n = 1,2,..,NODET \qquad 3.12$$

The geometric characteristics of each panel are essential for calculating the coefficients in the system of equations (Green's identity). Thus, each panel needs to be numbered for the formation of a data structure in the code and the control point coordinates, coordinates of the edges, surface area etc. are the variables of the structure.

The wake is gradually generated in time, as the flow develops and is considered as a vortex sheet (VLM), divided in the near and the far wake regions. The near wake is emitted in every time step from the trailing edges of the body. As stated before, the aim of this thesis is to research the characteristics of the flow around a bluff body and set the basis for an approximative formulation, so the exact flow pattern is not desired. Thus, for time efficiency reasons the simple case of wake emission from the rear edge is modelled, as presented in Figure 3.6. The near wake panels are formed by the extension lines of the body at the spanwise direction (y axis) and their length Δl_w is defined by the numerical parameters dt and $\mathbf{u}_{nw}$ that will be analyzed in Numerical Parameters. A general rule for this length is to have the same order of magnitude with the panels of the body at the vicinity of the trailing edge.

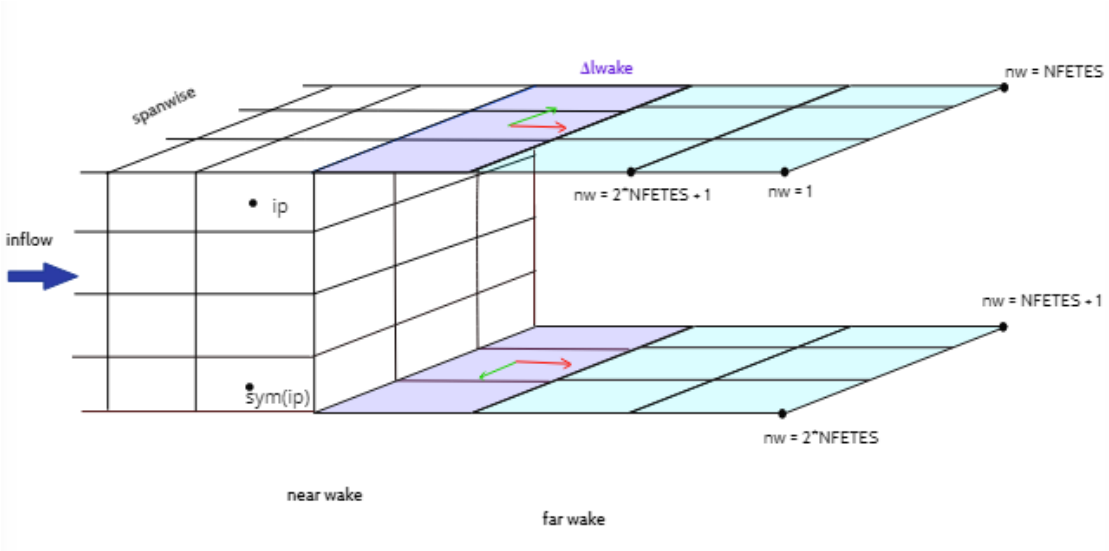

Figure 3.6: Wake discretization (VLM) & symmetrical panels

The count of the nodes defines the local coordinate system of the wake panels, as presented in the illustration figure above. Conversely to the body discretization that is constant in time, the wake nodes are moved at the end of each times step (free wake model) based on the Biot-Savart law. Hence, a free wake pattern is obtained. In the vortex particle method, the near wake and even a region of the far wake is modelled as a lattice.

Numerical Parameters

The emission velocity of the near wake from the trailing edge is $\mathbf{u}_{nw}$ and its direction is parallel to the upstream panel as presented in Figure 2.9. A general expression for this velocity is

$$\mathbf{u}_{nw} = \frac{\mathbf{u}^{+} + \mathbf{u}^{-}}{2} \tag{3.13}$$

The length of the wake panel is essential for the calculation of the near wake AIC and is given by

$$d\mathbf{l}_{w} = \mathbf{u}_{nw} dt \tag{3.14}$$

Thus, $\mathbf{u}_{nw}$ has to be specified before the numerical solution of the matrix and is considered a numerical parameter of the problem. A valid assumption is

$$\mathbf{u}_{nw} = \mathbf{U}_{\infty} \tag{3.15}$$

The timestep dt and the freestream velocity $\mathbf{U}_{\infty}$ are input parameters for the solution of the problem. An empirical rule for the selection of the timestep is the length of the near wake to be the same order of magnitude with the panels of the body near the trailing edge.

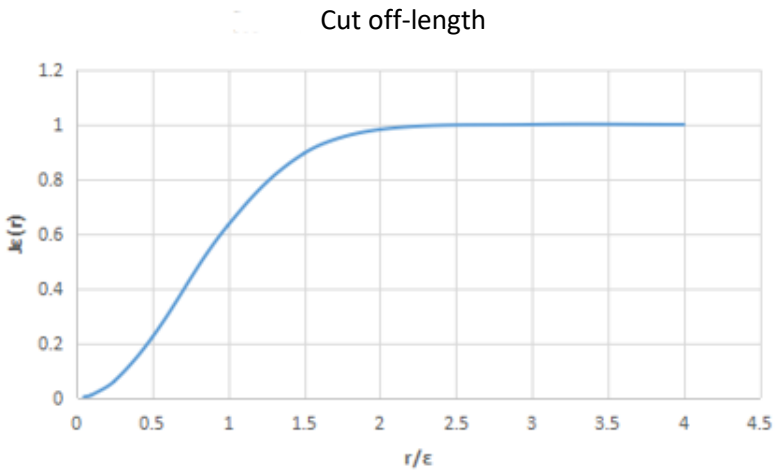

Figure 3.7: Mollifier function and cut-off length ε (vortex core radius)

$$J_{E(r)} = 1 - e^{-(\frac{r}{\varepsilon})^2} \tag{3.16}$$

The calculation of the velocity (Biot-Savart law) in an arbitrary point P of the flow field induced by a vortex element j (surface doublet) when the relative distance $r \to 0$ leads to a singularity. A mollifier function $J_{E(r)}$ Figure 3.7 is multiplied with the induced velocity in order to overcome the singularities that occur. In that way the velocities induced in points

close to the vortex core are normalized. In reality, the viscosity maintains the fluid particles consistent and moderates the strong effect of vorticity. The challenge in bluff body aerodynamic problems (thick wake) solved with inviscid methods is to find the right combination of numerical parameters that simulate the strong viscosity effects that characterise the extended separation zone.

Velocity Calculation

The analytical and numerical (Gauss Theorem) expression for the derivative of the velocity potential (constant Φ distributions $\rightarrow \nabla\Phi = 0$ along each panel dS) are presented in 3.17, 3.18 respectively.

$$\mathbf{u}(\mathbf{x}) = \frac{1}{4\pi}\oint \mu(\mathbf{s})\frac{d\mathbf{l}\times(\mathbf{x}-\mathbf{s})}{|\mathbf{x}-\mathbf{s}|^3} + \frac{1}{4\pi}\int_{S_B}\sigma(\mathbf{s})\left(\frac{(\mathbf{x}-\mathbf{s})}{|\mathbf{x}-\mathbf{s}|^3}\right)dS \tag{3.17}$$

$$\mathbf{u}(\mathbf{x}) = \frac{1}{\Delta D}\int_{\Delta S^e}\Phi(\mathbf{s})\cdot\mathbf{n}\,dS \tag{3.18}$$

Dimensionless Pressure Coefficient Cp

The pressure coefficient Cp is a dimensionless number that characterizes the flow and is essential in order to compare the results of similar aerodynamic problems with different parameters (aspect ratio, $\mathbf{U}_\infty$, dt, ε). The Cp number is used for the validation of a formulation when compared with results from experiments or alternative formulations.

$$C_p = \frac{p - p_\infty}{\frac{1}{2}\rho {U_\infty}^2} \tag{3.19}$$

The relative pressure $p - p_\infty$ at a point C of the flow field is calculated by applying the Bernoulli energy equation. As stated in Bernoulli Energy Equation, this equation represents the conservation of energy along a line that connects C with a point far from the flow field. In cases when point C lies in the viscid region and consequently the line intersects the wake surface, that divides the flow field in two zones (inviscid – recirculation) Figure 2.8, the residual of energy term Dh needs to be considered in the calculation of C_p.

$$\frac{\partial\Phi_c}{\partial t} + \frac{p_c}{\rho} + \frac{{\mathbf{U}_c}^2}{2} + Dh = \frac{\partial\Phi_\infty}{\partial t} + \frac{p_\infty}{\rho} + \frac{{\mathbf{U}_\infty}^2}{2} \tag{3.20}$$

The region far from the flow field remains undisturbed so the unsteady term $\frac{\partial\Phi_\infty}{\partial t}$ is set to zero. The discretized form of the above equation for a timestep and for i indicating a point in the flow.

$$p_i - p_\infty = \rho\left(\frac{{\mathbf{U}_\infty}^2}{2} - \frac{{\mathbf{U}_i}^2}{2} - \frac{\Phi_i - \Phi_i^{(t-Dt)}}{Dt} - Dh_j^{(1dt)}\right), \quad j = 1,2,..,NPANW \tag{3.21}$$

$$\mathbf{x}_i \in S_{inviscid} \rightarrow Dh_j^{(1dt)} = 0$$

4. Results

The aim of this thesis is to investigate the validity of panel method algorithms for the approximative solution of bluff body aerodynamic problems. From the results presented in this section, the characteristics of the flow around bluff geometries are analyzed and the assumptions made are evaluated. The validation of the results is held through comparison with experimental data and CFD (viscid) methods.

The external flow conditions and the dimensions of the building model examined will be the same with existing experiments (Model 2) in order to compare the results and validate the accuracy of the direct formulation. The atmospheric boundary layer is characterized by the unsteady stochastic phenomenon of turbulence and a transverse gradient of the horizontal velocity component u at the z direction that represents the viscosity effects near the solid ground and satisfies the no slip boundary condition

This formulation is an approximate method and turbulence modelling will not be included. The distribution of the boundary elements at the surface of the model, eliminates significantly the DOFs of the problem. The mesh consists only of the discretized model in contradiction to the classic Navier- Stokes method where the mesh consists of the body and a space that surrounds it which extends at a distance approximately 10H from the body. The fundamental difference of the two methods is the specification of the flow field (Lagrangian vs Euler).

In the validation stage, the distribution of $\mathbf{U}_{\infty}(\mathrm{z})$ will be chosen to be constant in order to neglect the atmospheric boundary layer. As will be shown below, because of the extended thickness of the ABL compared to the height of the building, this assumption is not a valid simulation of the physical problem. Thus, a distribution of $\mathbf{U}_{\infty}(\mathrm{z})$ that corresponds to experimental data will be chosen as input to the problem.

As presented in Alternative Formulations two alternative methods are examined in this thesis based on the direct formulation (Morino & Kuo). The results of parametric analysis (cut off length, aspect ratio, dt) will be presented in this section.

The distributions of the flow characteristics (Cp, U) along the body presented below refer to the central path of the body and Model1.

Model1	
D(m) – x direction	0.125
H(m) – z direction	0.100
B(m) – y direction	0.150
U_{∞} (m/s)	4.5

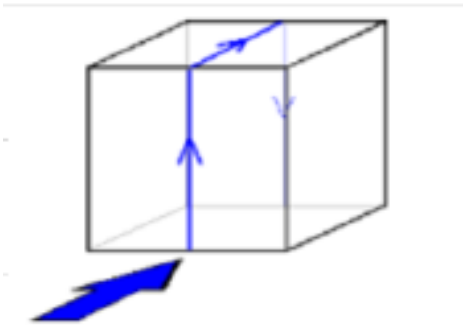

Figure 4.1: Central path y=0 *(13)*

Grid Independence

The optimum density of the mesh combines grid independence and the minimum number of nodes in order to achieve reduction of the computational cost and accuracy of the solution. A general rule in computational mechanics is to increase the density of the grid in regions of high gradients. A characteristic of this rectangular shape that needs to be taken into account is the behaviour of the inviscid flow around the sharp-edge which tends to an infinite velocity in this region. Based on the above fact, grid independence cannot be achieved so at first a uniform grid is used in an ideal (potential) steady flow simulation without a wake model.

In the grid independence simulations, Formulation 1 is applied to the solution of the flow. Formulation 2, cannot correspond to the steady potential flow problem since it is based on the physics of bluff body aerodynamics which is characterized by the unsteady separation phenomenon (wake model cannot be neglected).

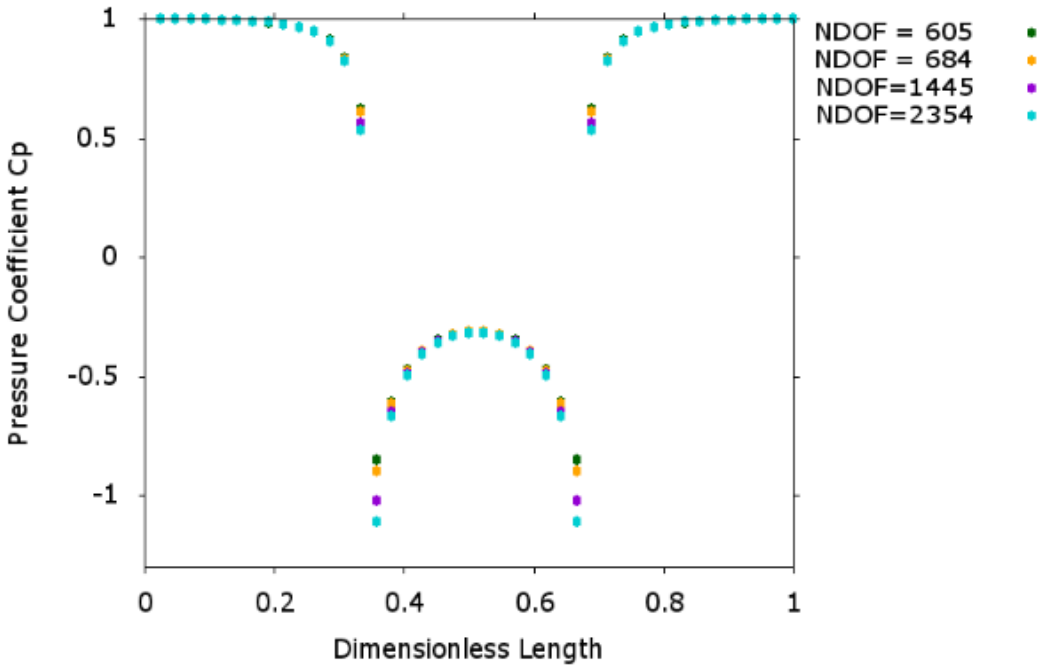

Figure 4.2: Grid Independence at the steady state – potential flow

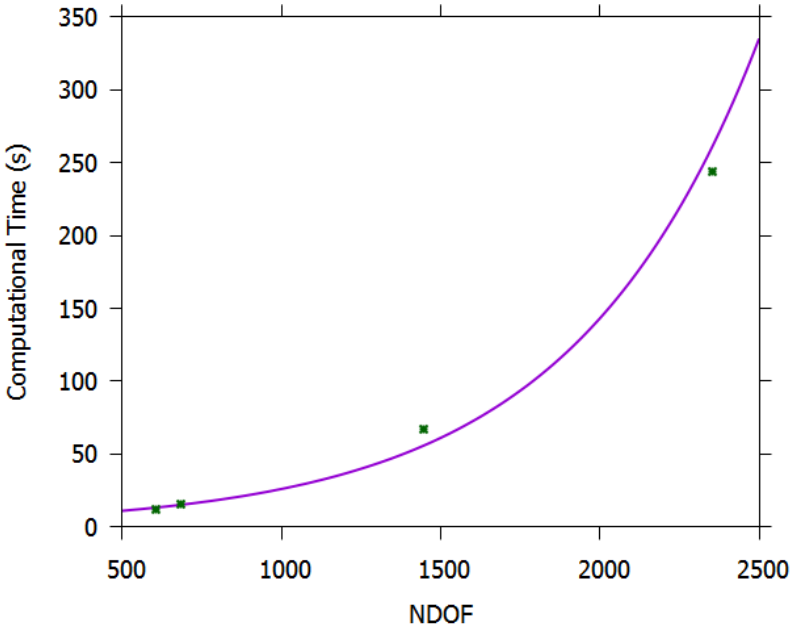

Figure 4.3: Exponential increase of the computational time (1 dt) depending on the DOF's

The panels of the body in the simulations presented in this chapter and for Model1 are NPANB = 1484.

Symmetrical Solutions

The main interest of this thesis is the specification of the flow pattern of the unsteady problem and an approximative solution is desired. Thus, the structure of a numerical system with reduced DOF's is essential. The assumption of the symmetrical solutions 3.4 is valid (before the instabilities of the wake occur) (Vortex shedding) as presented in the figures bellow. By using the equivalent symmetrical system for the solution, the DOF's are reduced to the half leading to a significant reduction of the computational time Figure 4.3. The vortex shedding phenomenon (non-symmetric solution) develops after the roll up of the wake.

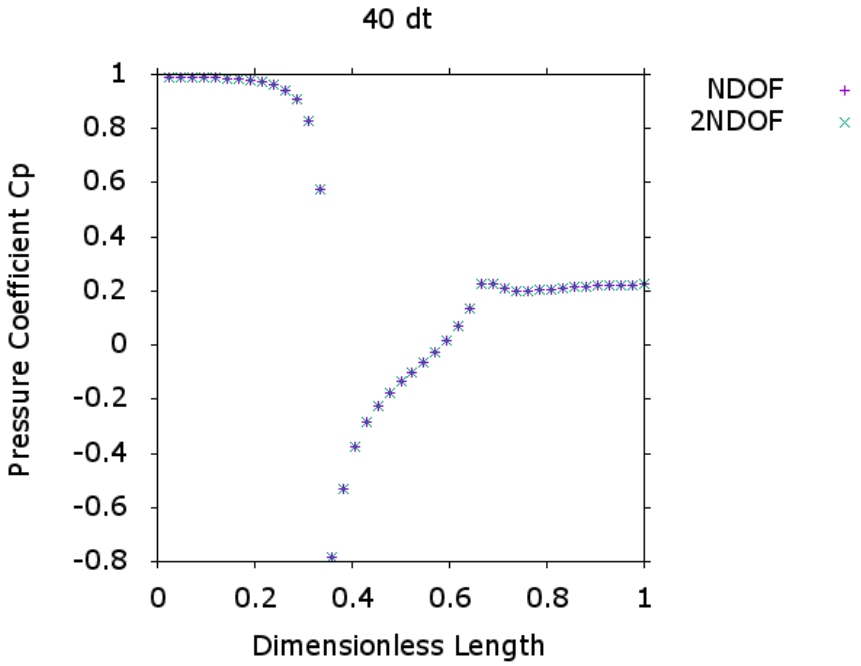

Figure 4.4: Formulation 2

Separation characteristics (Form1)

In Figure 4.5 the expected stagnation of the velocity at the panel (y=0) downstream the trailing edge occurs for a simulation of 30 dt. At the central panel the symmetrical flow has 2D characteristics and thus the velocity at the t direction(crossflow) is zero. The unsteady nature of the problem and the generation of the wake at every time step makes the observation of the flow development from t = 0 s until the steady state essential.

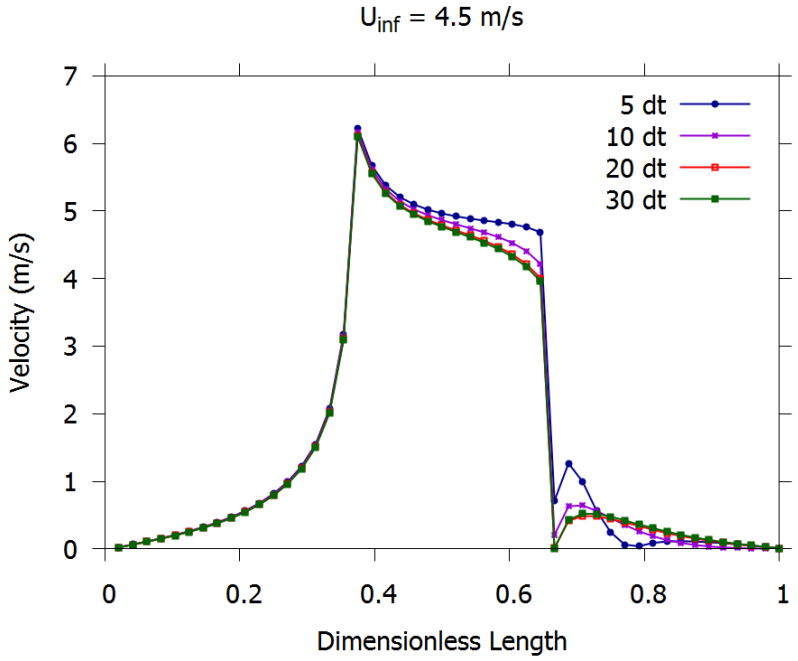

Figure 4.5: Stagnation downstream occurs as the flow develops

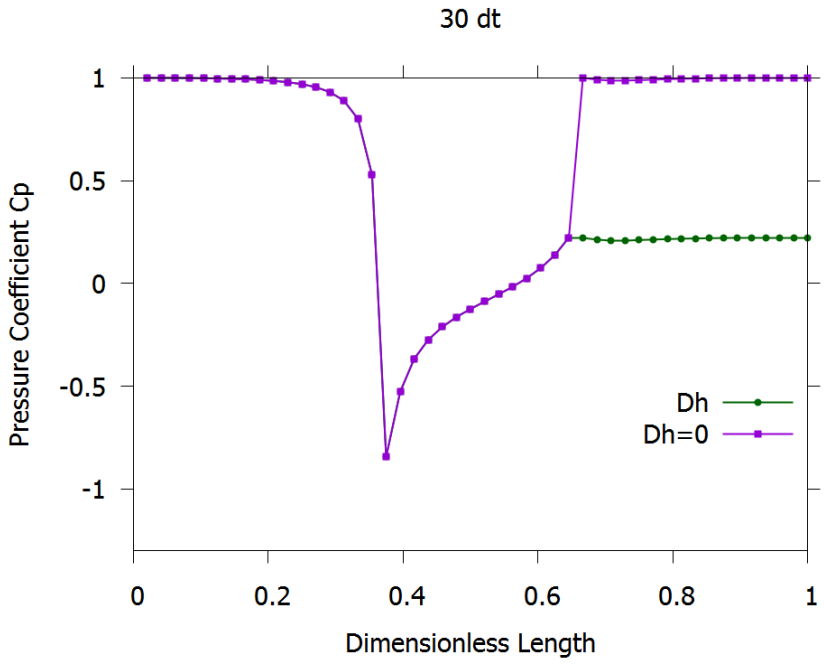

Figure 4.6: Effect of energy residual Dh on Cp (20 dt)

As presented in the Cp distribution above, the incorporation of the residual of energy Dh (3.20) at the viscid region, is consistent with the Kutta Condition for the incompressible fluid at the TE.

Comparison of formulations

Formulation 2 imposes the stagnation on the first row of panels downstream the trailing edge and the vorticity shed on the wake $\|\Phi\|_w$ is considered unknown for the solution of the system. The two formulations yield to similar results after the stagnation at the downstream row of panels (Figure 4.5).

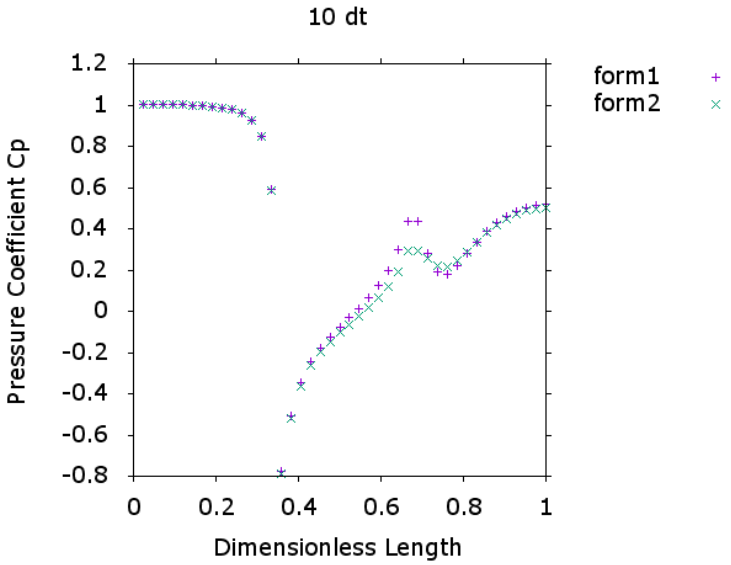

Figure 4.7

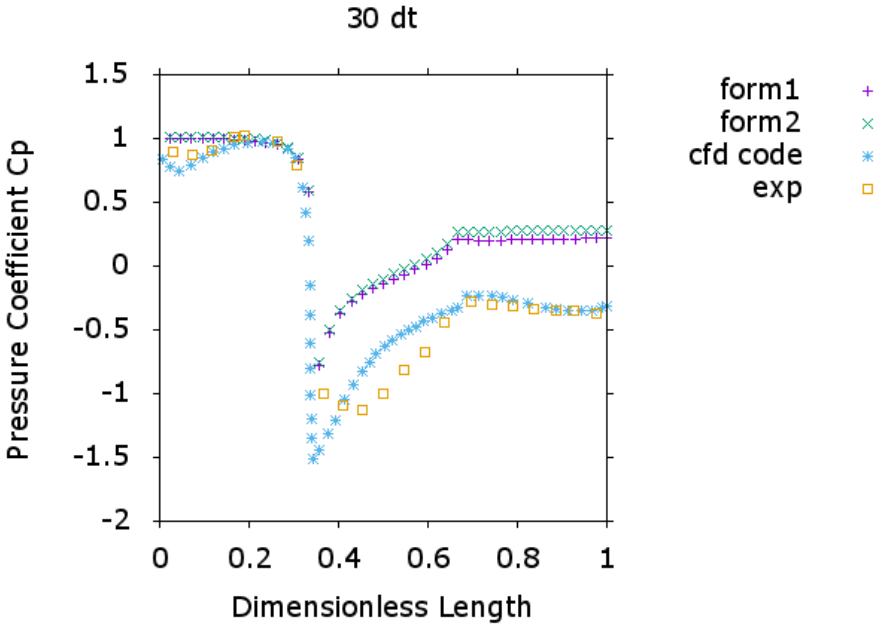

Figure 4.8: Comparison of formulations with CFD (3) and experimental simulations (5)

Cut off length analysis

The vortex core radius ε (cut off length) is a parameter that determines the effect of vorticity induced a vortex segment. In Figure 3.7, the smoothing rate of the induced velocity at a point, which is at distance r from the vortex segment, is presented depending on the $\frac{r}{\varepsilon}$. The results of the cut off length analysis confirm the importance of this parameter for the wake pattern and the flow field at the viscid region.

Formulation	2
dl_w/dx	1
$u_w = u_{inf}$ (m/s)	5
$dt = dl_w/u_w$ (s)	0.0014
Timesteps	50

Table 4.1: Conditions of cut off length analysis simulation

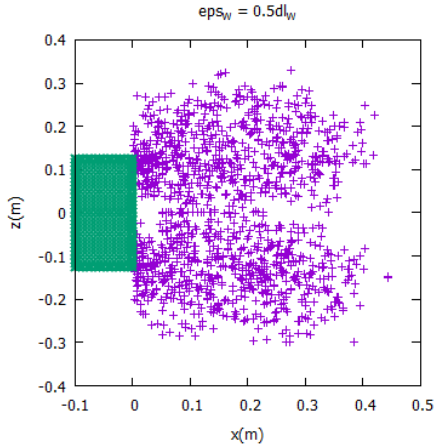

Figure 4.9

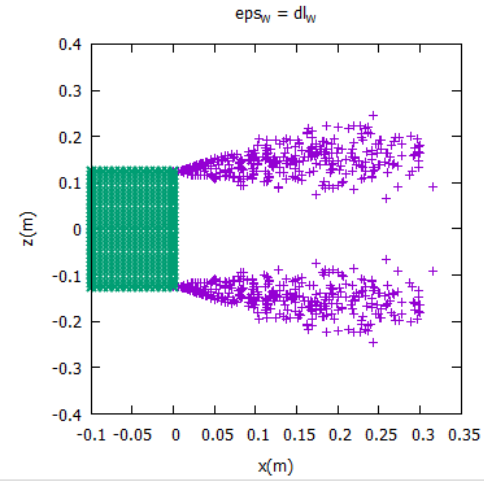

Figure 4.10

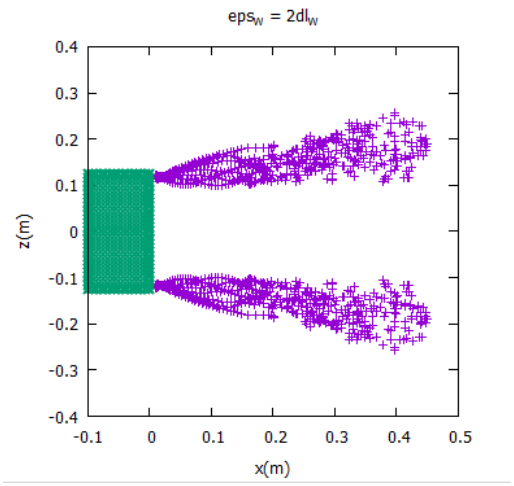

Figure 4.11

The wake pattern that corresponds to ε = $0.5\,\mathrm{dl_w}$ is inconsistent with the real physics problem, as the wake surface has no continuity which is contrary to the presence of viscosity. Even if the method is inviscid, the physical norms cannot be contradicted. Thus, a smaller effect of the vorticity induced by the doublet elements that model the wake surface needs to be chosen. The expected wake pattern (separation bubble) is illustrated in Figure 2.8. In Figure 4.11 , the effect of vorticity ε = $2\mathrm{dl_w}$ is underestimated and the solution declines from the real problem. In order to obtain the effect of the wake on the flow field, the Biot-Savart law is applied for the calculation of the velocities. The velocity profiles for y=0 are presented below for three positions downstream the body (x=0.01, x=0.05, x=0.1) and compared with the potential flow results. The different effect of wake vorticity is addressed through parameter d = $\frac{\varepsilon}{\mathrm{dl_w}}$.

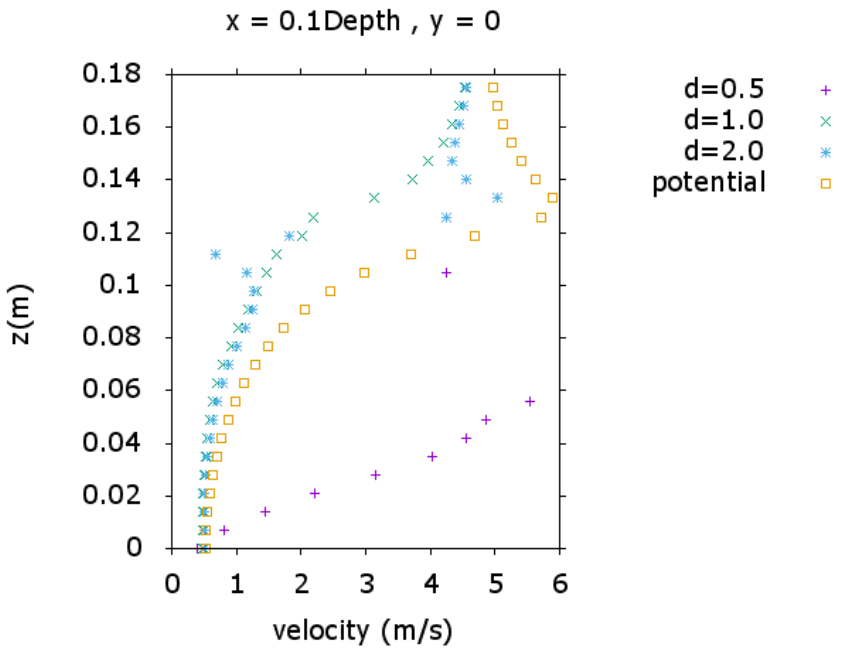

Figure 4.12

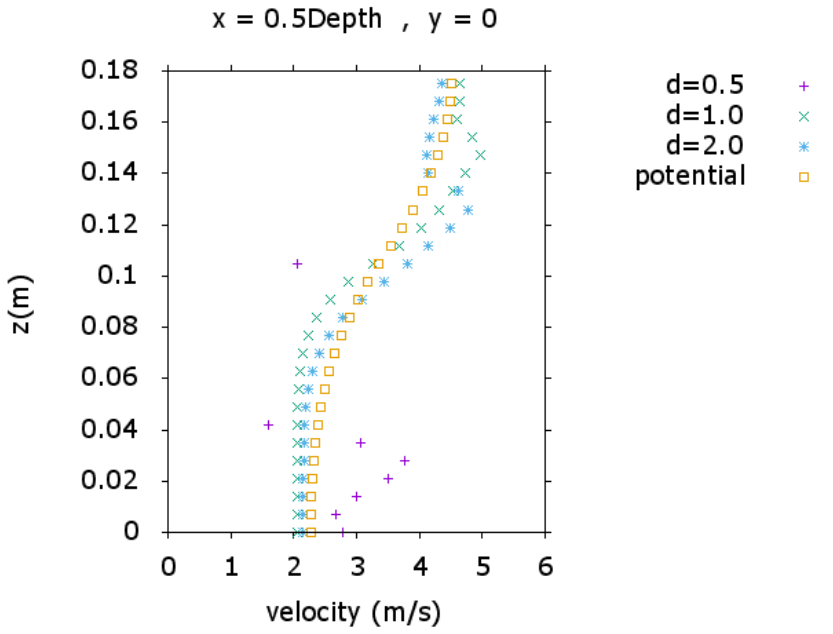

Figure 4.13

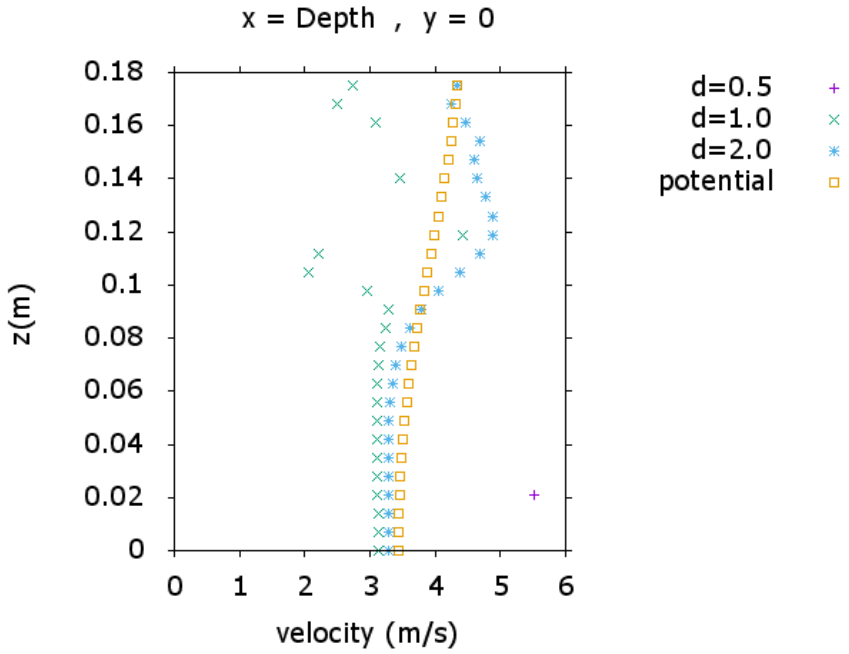

Figure 4.14

Flow Field

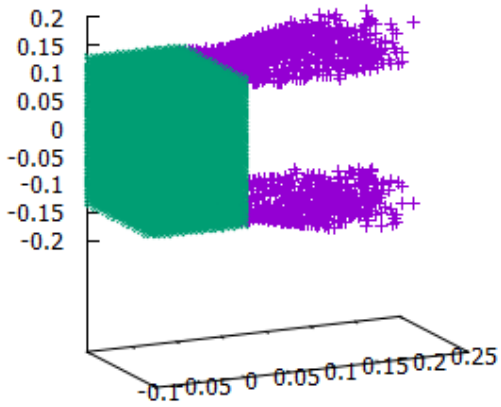

Figure 4.15: Wake topology at 30 timesteps

The calculated velocity distribution along the z direction (Biot-Savart law) is compared with the potential flow and CFD (4) results at the same position. The results are compared only in the vicinity of the near wake, since the desired recirculation region has not been generated (simulations of more than 30 timesteps have been held).

The VPM method at the height of the building Z=0.125 yields a similar result with the CFD simulation and the desired cancelation of the potential acceleration is achieved.

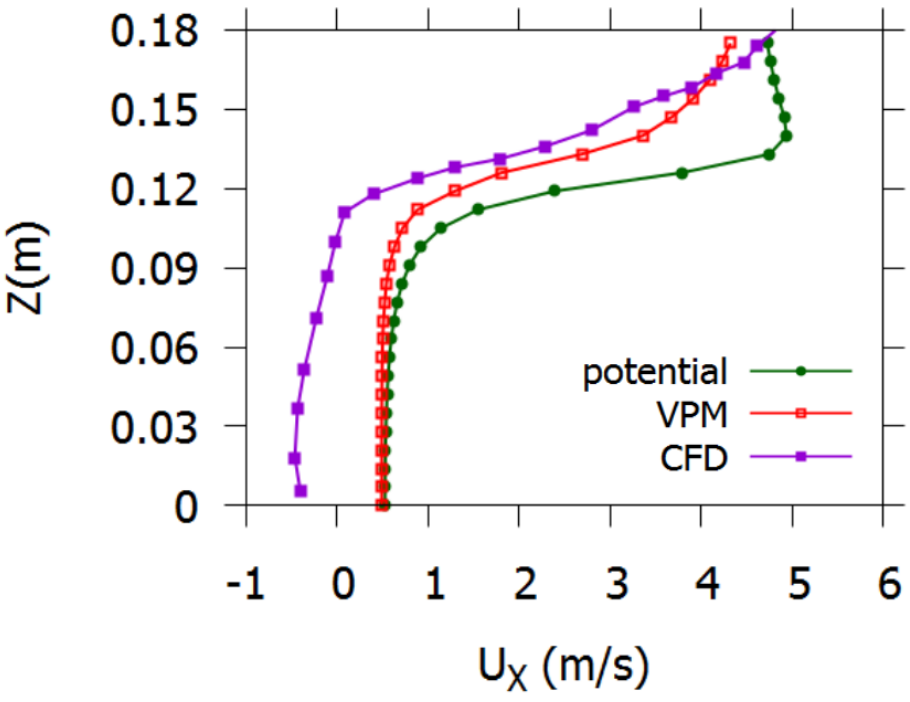

Figure 4.16: Downstream velocity distribution at the vicinity of the near wake (x=0.1D, y=0)

Incorporation of ABL (Atmospheric Boundary Layer)

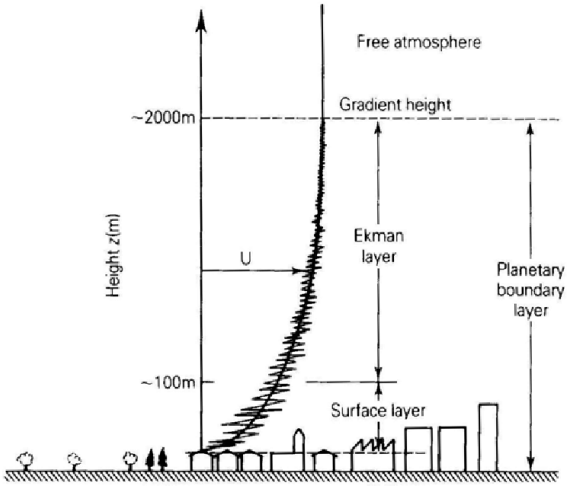

Figure 4.17: At the height of buildings a strong transverse gradient of $U_{\infty x}$ occurs

As presented in the illustration above, the freestream velocity is not constant along the height of the body. Despite the fact that the turbulence and viscosity terms of the ABL are not part of the inviscid method, a velocity profile $U_{\infty x}$ (z) will be incorporated as input for the code for a better approach of the real problem.

Model2	
D(m) – x direction	0.110
H(m) – z direction	0.110
B(m) – y direction	0.110

Table 4.2: Uwake = 3.5 m/s

For the validation of the ABL simulation, the results are compared to CFD (3) and experimental (5) simulations. Thus, the input vertical velocity distribution corresponds to the ABL profile used in the latter cases and is estimated by the log wind profile that characterizes the surface layer.

$$U_{\infty x}(z) = \frac{u*}{\kappa}\ln\left(\frac{z}{z_o}\right) \qquad 4.1$$

Parameter	Description	Low shear (case 4a)	High shear (case 4b)
z_o(mm)	surface roughness	0.05	0.7
u*(m/s)	friction velocity	0.19	0.27
K	Von Kaarman constant	0.41	0.41

Table 4.3: Log wind profile parameters

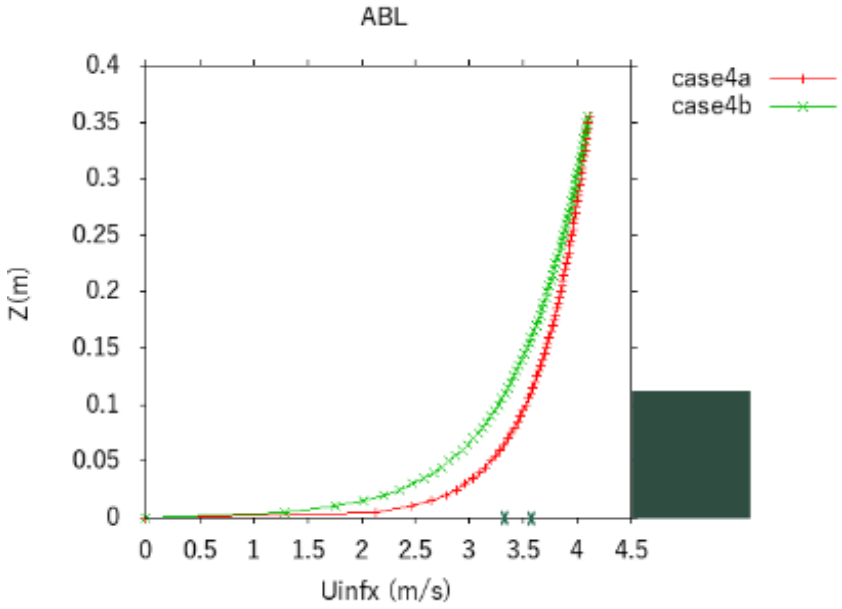

Figure 4.18: Input $U_\infty = U_\infty x(z)$ and near wake emission $u_{nw} = U_\infty x(z = H)$

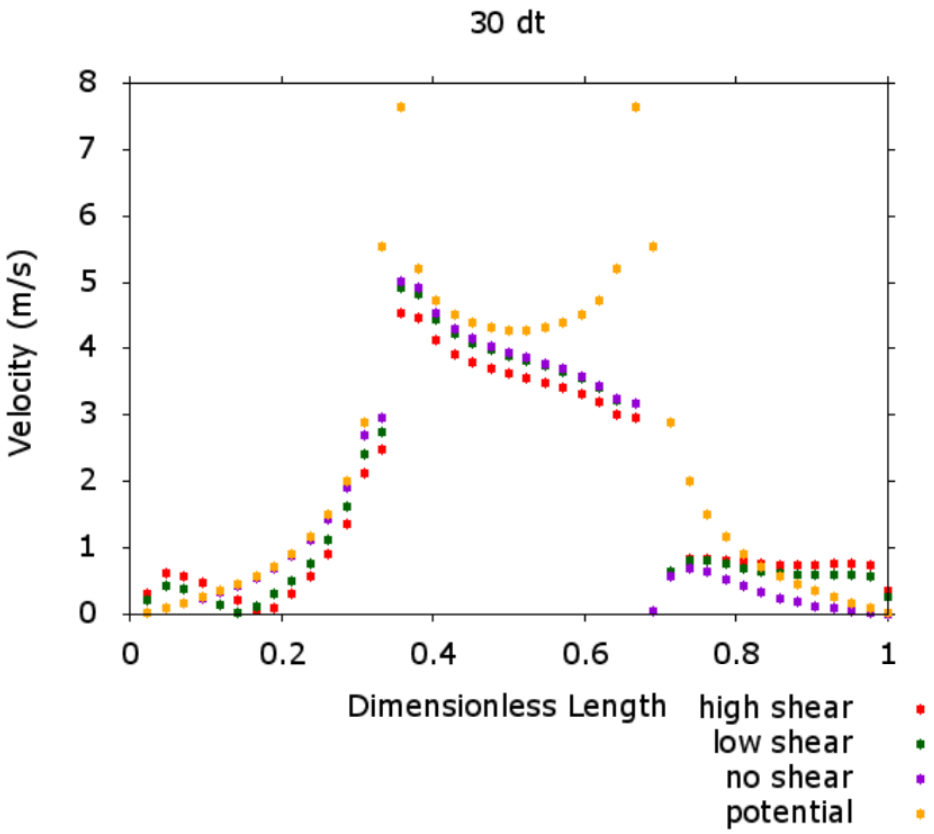

Figure 4.19

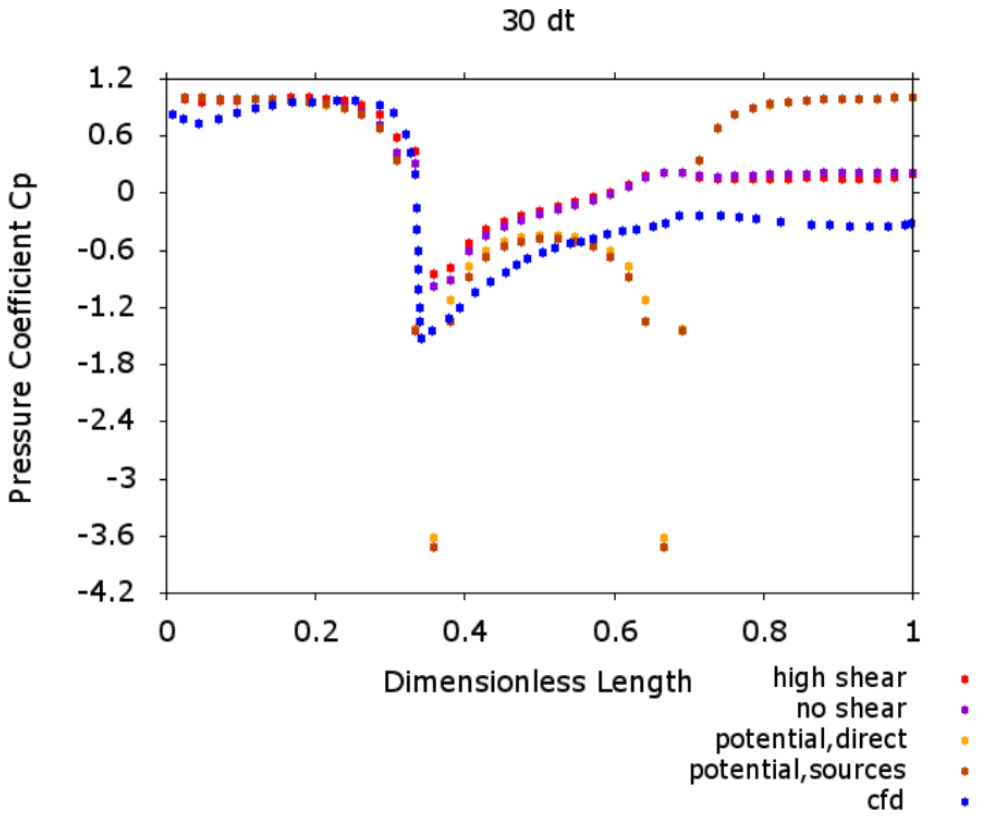

Figure 4.20: $U_\infty = U_{\infty x}(H)$ for Cp

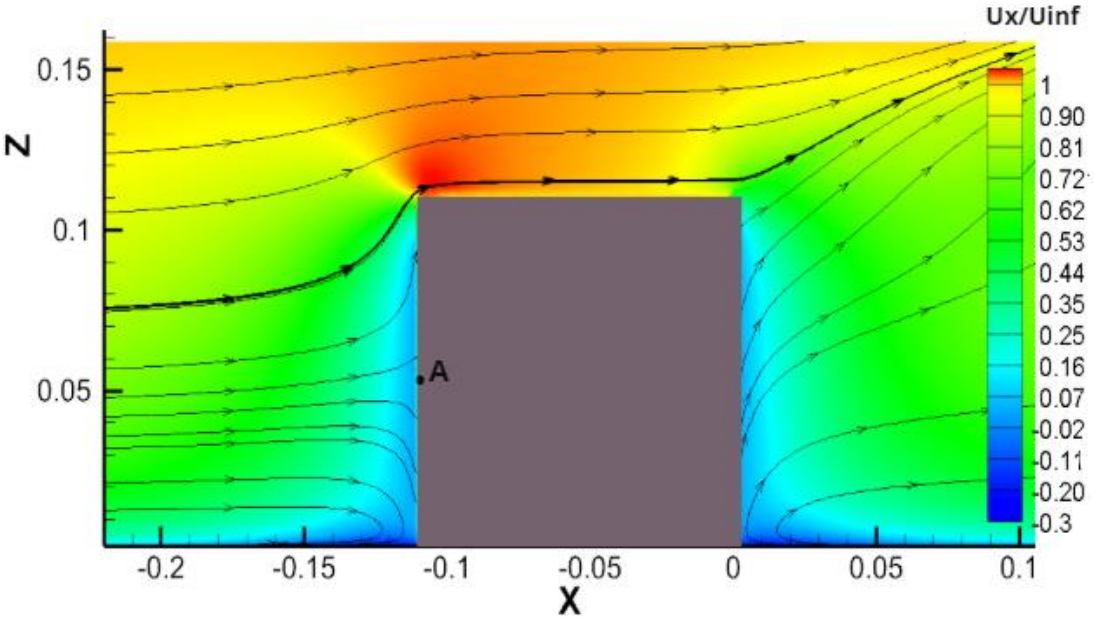

Figure 4.21: high shear, steady state 30 dt, y=0

As presented in the figures above, the incorporation of a $U_{\infty}x(z)$ in the code does not affect the pressure distribution significantly, since the viscous and turbulent terms that characterize the ABL are neglected in the inviscid method. Despite the later fact, an improvement of the method is achieved as the stagnation point in the front plane is shifted from the ground (z=0) to point A, which occurs in the real flow around a building.

Miscalculation of velocities

The pattern of the Cp distribution is similar with the experimental data and the results of the CFD simulation (Figure 4.8), but the deviation is significant even for an approximative method. Thus, in order to identify the root of the deviation and to obtain a valid solution, if possible, the assumptions of the method need to be investigated. As presented in Figure 3.2, a constant distribution of the surface elements (σ, μ) along the panels is chosen. The doublet elements are placed in the surface of the body for the generation of vorticity. Therefore, the potential flow case can be modelled by adjusting only source distributions at the boundary S_B. This formulation is consistent with the symmetrical geometry of the bluff body. In reality, despite the symmetrical geometry, circulation occurs due to flow separation at the edges of the body (D 'Alembert Paradox).

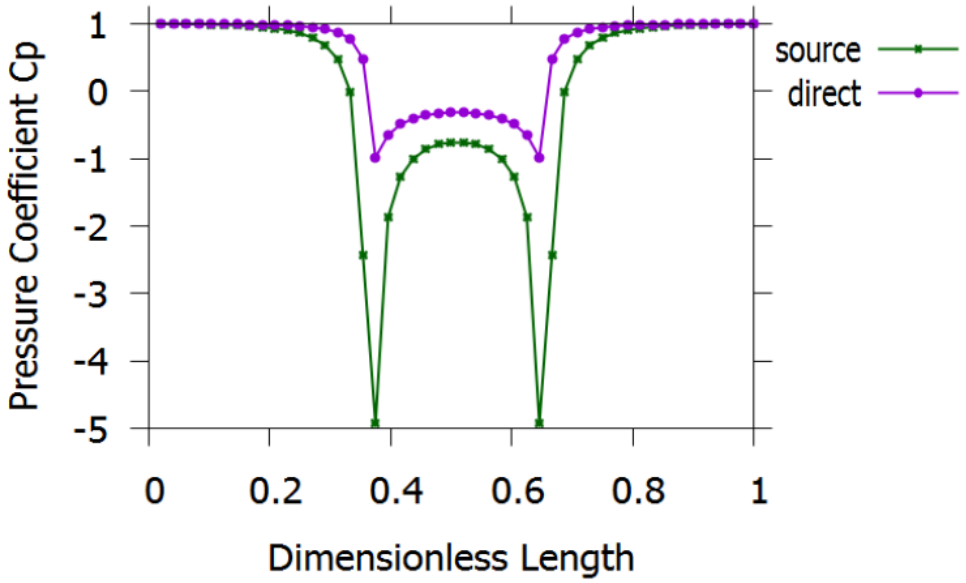

Figure 4.22: Miscalculation of velocity due to the doublet constant distributions

It is obvious that the discontinuities on the nodes of the body that occur due to the constant distribution assumption are inconsistent with the physics of the problem due to the neglection of the surface vorticity on the calculation of velocity. The correct velocity calculation can be achieved by a linear interpolation of the constant potential distribution (direct approach $\mu_B = -\Phi$) at the body nodes after the algebraic system is solved (Neumann boundary condition **U**·**n** = 0 at collocation points) at each timestep.

5. Conclusions

The most important observations from the method developed are listed bellow

- Stagnation point at the front plane shifts from ground to A and reversed flow upstream occurs with the incorporation of ABL as a $U_\infty x(z)$ distribution. Figure 4.21
- Desired constant pressure distribution at rear plane (Separated flow region) Figure 4.20
- Improvement of the potential flow Figure 4.16,Figure 4.20.
- An interpolation of the potential from the collocation points to the surface nodes is essential for the correct calculation of the velocity Figure 4.22
- From the results of the CFD simulation it seems that the separation that affects significantly the pressure field upstream is from the rear edge (wake model). In reality the flow separates from the front and side edges due to the sharp corner but the presence of a solid surface aligned with the free stream leads to a reattachment of the flow. Despite the recirculation that occurs in these surfaces, because of its limited area its behavior is similar to an attached boundary layer as far as the Cp distribution is concerned. This is the reason the Cp distributions are similar even if no wake is emitted from the front and side edges at the simulation of the code developed in this thesis. Of course, the strong turbulence that occurs in these regions, which is neglected in the inviscid method, yields a different Cp pattern as presented in the experimental results in Figure 4.8.

As presented in Figure 4.20 although the Cp pattern is the same with the results from the CFD simulation, the distribution is shifted and the desired suction at the rear plane is not obtained. This observation combined with the fact that the expected recirculation region (bubble downstream) could not be generated leads to the assumption that the deviation from the expected results is probably due to the miscalculation of the circulation shed on the wake. It is important to note that expected stagnation at the first row of panels downstream the trailing edge occurs with Formulation1 (Figure 4.5).

Recommended ***cases for future investigation***

- The interpolation of the potential from the collocation points of the body (Neumann boundary condition) at the nodes is an essential issue to be resolved for an accurate calculation of the velocity. The stagnation condition presented in Formulation 2 can be used in order to define the potential of the downstream node Φ^-.

$$\Phi^- = \frac{1}{2}(\Phi_{\text{ipdn}} - \Phi_{\text{ipdn+1}})$$

- The region of the vortex lattice that represents the far wake can be converted to vortex particles. In cases of wake roll up (strong vorticity) the lattice may be deformed and thus numerical instabilities occur. The modelling of the far wake area with particles is preferable for simulating a turbulent flow. An important advantage of this conversion, is the reduction of the computational cost since the point vortices can be merged into groups.

- Rearrangement of the domain. The definition of the problem can be made based on the flow separation and the division of the flow field in an inviscid and viscid region Figure 5.1.

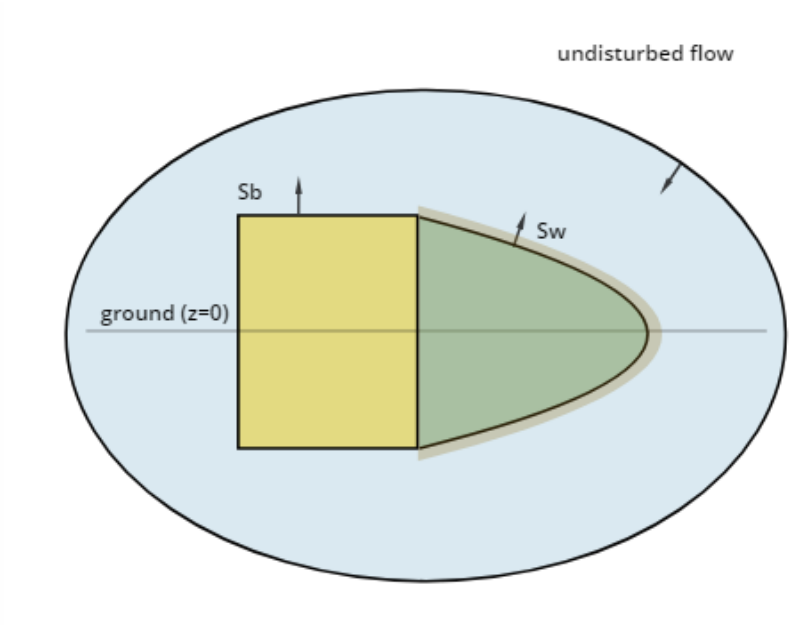

Figure 5.1: Rearrangement of the domain

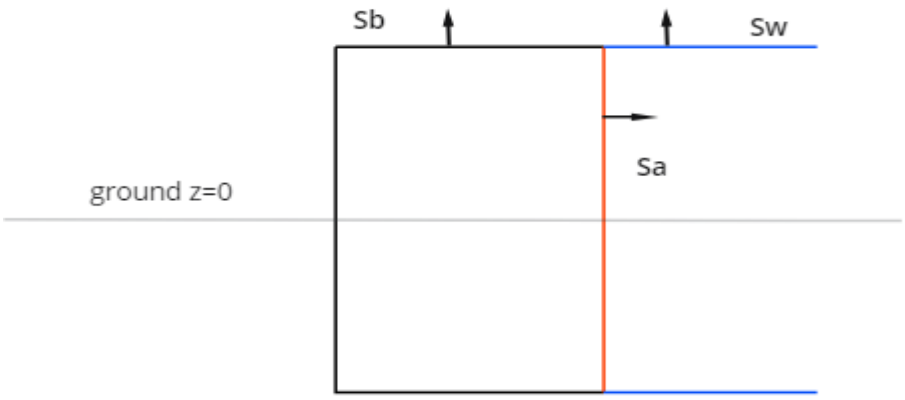

Figure 5.2: Different element distribution in Sa, Sb, Sw depending on the physics of the region

References

1. **Buresti, G.** Vortex shedding from bluff bodies. *Wind Effects on Buildings and Structures.* Rotterdam : Riera J.D., Davenport A.G., Eds., 1998, 4.

2. *Unsteady RANS modelling of flow past a rectangular cylinder: Investigation of Reynolds number effects.* **Mannini, Claudio, Soda, Ante and Schewe, Gunter.** 2010, Computers & Fluids, p. 16.

3. *Computational Simulation of a Building Embedded in the Atmospheric Boundary Layer.* **Kalogeraki, Anastasia.** 2018.

4. **Gousdovas, Konstantinos.** *Αριθμητική προσομοίωση ατμοσφαιρικής ροής και διαποράς ρύπου γύρω από πρότυπο κτίριο.* Αθήνα : Μεταπτυχιακή Εργασία, ΔΠΜΣ Υπολογιστκή Μηχανική, 2018.

5. **Meletis, Panos.** *Πειραματική προσομοίωση πρότυπου κτιρίου εκτεθειμένου σε ατμοσφαιρικό οριακό στρώμα.* Αθηνα : Διπλωματική εργασία, Σχολή Μηχανολόγων Μηχανικών ΕΜΠ, 2017.

6. **Katz, Joseph and Plotkin , Allen.** *Low Speed Aerodynamics.* 2. San Diego, US : Cambridge University Press, 2001.

7. *Development of Free Vortex Wake Method for Aerodynamic Loads on Rotor Blades.* **Abedi, Hamidreza, Davidson, Lars and Voutsinas, Spyros.**

8. **Riziotis, Vasilis and Voutsinas, Spyros.** Dynamic stall modelling on airfoils based on strong viscous-inviscid interaction coupling. 2008.

9. *A Viscous-Invoscid Interaction Model for Dynamic Stall Simulation on Airfoils.* **Voutsinas, S.G and Riziotis, V.A.** Reno : s.n., 1999. 37th Aerospace Sciences Meeting and Exhibit.

10. **Zou , F, et al.** Analysis of vortex and stall induced vibrations at standstill conditions using a free wake aerodynamic code. *J Wind Energy.* 2015, Vol. 18, 12.

11. **Riziotis, Vasilis.** *Αεροδυναμική και Αεροελαστική Ανάλυση της Απώλειας Στήριξης σε Δρομείς Ανεμογεννητριών.* Αθήνα : Τομέας Ρευστών ΕΜΠ, 2003. PhD.

12. **Kato, Naomi.** *A study on Separated Flows behind Bluff Bodies by Inviscid Vortex Model.* 1982.

13. *Experimental Study of the Flow past a Cube wirh Openings Embedded in a Turbulent Boundary Layer.* **Manolesos, Marinos, et al.** Chicago,USA : s.n., 2017. 10th International Symposium on Turbulence and Shear Flow Phenomena.

14. **Riziotis, Vasilis.** *Aerodynamic and Aeroelastic Analysis for the Stall FLutter in Wind Turbines, PhD.* 2003.

Εκτενής ελληνική περίληψη

ΕΙΣΑΓΩΓΗ

Η αεροδυναμική μελέτη κτιρίων είναι χρήσιμη για τον υπολογισμό της κατανομής πίεσης επί της επιφάνειας τους και συνεπώς των ασκούμενων φορτίων (αντοχή,διείσδυση αέρα..). Επίσης είναι απαραίτητη σε επίπεδο πόλης για λόγους άνεσης και για εκτίμηση των ρευμάτων σε υψηλούς ανέμους. Κατά την κατασκευή κτιρίων μεγάλων διαστάσεων είναι απαραίτητος ο υπολογισμός της επίδρασης του vortex shedding, καθώς το φαινόμενο μπορεί να οδηγήσει το κτίριο σε συντονισμό και σε ακραίες περιπτώσεις αστοχία. Τέλος, η προσομοίωση της ροής γύρω από κτίριο χρειάζεται σε προβλήματα όπου υπάρχει αλληλεπίδραση δρομέα με την κατασκεύη, όπως πχ ελικόπτερο που εκτελεί χαμηλή πτήση. Στην τελευταία περίπτωση, που είναι η εξεταζόμενη της διπλωματικής, αρκεί μια προσεγγιστική λύση της ροής, δηλαδή να προκύψει διακριτή ζώνη αποκόλλησης για τον υπολογισμό των ασκούμενων πιέσεων και όχι το ακριβές πεδίο ροής.

Το κτίριο μοντελοποιείται με σώμα κυβικής γεωμετρίας που θεωρείται μη αεροδυναμικό (bluff body). Ως μη αεροδυναμικά χαρακτηρίζονται τα σώματα που εξαιτίας της γεωμετρίας τους προκαλούν αποκόλληση της ροής από τις ακμές. Το αποκολλημένο τμήμα της ροής προσκολλάται σε μεγάλο μέρος της επιφάνειας τους (separation bubble) με αποτέλεσμα τον σχηματισμό ζώνης ανακυκλοφορίας (Figure *0.1*). Η προσκόλληση αυτή οφείλεται στις συνεκτικές δυνάμεις που συγκρατούν τα στοιχεία του ρευστού και δεν επιτρέπουν την μεταφορά τους και την διάλυση-απόσβεση (dissipation) των δινών αποκόλλησης. Στο πεδίο γύρω από αυτά τα σώματα εμφανίζεται διακριτό όριο μεταξύ συνεκτικής - μη συνεκτικής περιοχής . Σε μη συνεκτικές μεθοδολογίες απαιτείται λεπτή διαχείρηση αυτής της ζώνης και η μετάβαση από την μια περιοχή στην άλλη πρέπει να μοντελοποιηθεί κατάλληλα. Οι αναλογίες των διαστάσεων του ορθογωνικού 3D σώματος παίζουν καθοριστικό ρόλο στην γεωμετρία της ζώνης αποκόλλησης.

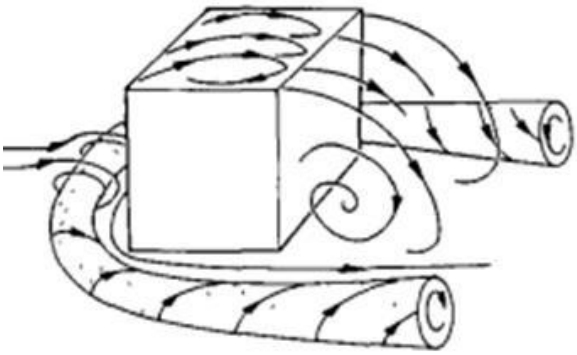

Figure 0.1: Ζώνες ανακυκλοφορίας λόγω αποκόλλησης

Σε σώματα όπως η σφαίρα και ο κύβος για την ιδανική περίπτωση όπου παρουσιάζουν αεροδυναμική συμπεριφορά, δηλαδή η ροή θεωρείται ασυμπίεστη,μη

συνεκτική και αστρόβιλη, λόγω της συμμετρίας τους ισχύει $\Gamma_{body} = 0$ και $F_{DRAG} = 0$. Όμως από πειραματικά δεδομένα για ροές σε μεγάλους αριθμούς Re, όπου οι συνεκτικές δυνάμεις μπορούν να αμεληθούν, προκύπτει πως σε αυτά τα σώματα ασκείται σημαντική F_{DRAG}. Αυτή η φυσική αντίφαση ονομάζεται παράδοξο D'Alembert και εκφράσθηκε το 1752 από τον ομώνυμο Γάλλο μαθηματικό.

Το παραπάνω φυσικό παράδοξο εξηγείται από την αποκόλληση της ροής που εμφανίζεται σε τέτοιου είδους γεωμετρίες. Η αποκόλληση της ροής αποτελεί φαινόμενο συνεκτικό. Ως οριακό στρώμα ορίζεται η λεπτή περιοχή κοντά στο στερεό όριο όπου η επίδραση της συνεκτικότητας δεν είναι αμελητέα και εντοπίζεται στροβιλότητα κοντά στην επιφάνεια του σώματος. Όταν εμφανίζεται μεγάλη κλίση πίεσης dp/dx, εκτός από περιπτώσεις πολύ συνεκτικών ρευστών, προκαλείται η αντιστροφή της ροής στην περιοχή εντός του οριακού στρώματος κοντά στο στερεό όριο. Το σημείο αποκόλλησης της ροής είναι εκείνο στο οποίο συγκρούονται οι ροές των δύο αντίθετων κατευθύνσεων επί της στερεής επιφάνειας, με αποτέλεσμα να εξαναγκαζεται το ρευστό να κινηθεί κάθετα στο στερεό όριο, αλλά στην πραγματικότητα το σημείο αποκόλλησης αποτελεί σημείο ανακοπής (mini stagnation point). Τα τυρβώδη οριακά στρώματα παρουσιάζουν μεγαλύτερη αντίσταση στην εμφάνιση της αποκόλλησης από τα στρωτά, καθώς λόγω της έντονης ανάμειξης μεταφέρεται κινητική ενέργεια προς το στερεό όριο καθυστερώντας την αντιστροφή της ροής.

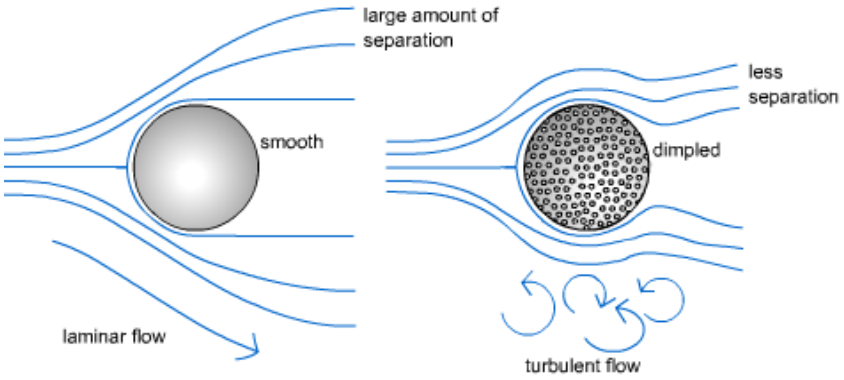

Figure 0.2: Τυρβώδες οριακό στρώμα → περιορισμός αποκολλημένης περιοχής → μείωση οπισθέλκουσας F_{DRAG}

Εκτός από την αποκόλληση που εμφανίζεται σε σώματα μη αεροδυναμικής γεωμετρίας, ένα άλλο χαρακτηριστικό της ροής είναι το vortex shedding, το οποίο παρατήρησε ο Von Karman. Αποτελεί περιοδικό φαινόμενο και περιγράφεται ως εναλασσσόμενη αποβολή στροβίλων αντίθετης έντασης από τις ακμές του σώματος. Η μελέτη αυτής της ταλαντούμενης ροής είναι κρίσιμη κατά την αεροδυναμική επίλυση κτιριακών δομών, καθώς η κατασκευή μπορεί να οδηγηθεί σε συντονισμό. Ο αδιάστατος αριθμός Strouhal αποτελεί μέτρο της περιοδικότητας και όπως φαίνεται από την παρακάτω σχέση εξαρτάται από τον Re. Μια σημαντική παρατήρηση είναι ότι η η ιδιότητα της συνεκτικότητας του ρευστού δεν λαμβάνεται υπόψιν στην παρακάτω σχέση :

$$St = \frac{fH}{U_\infty} \qquad 0.1$$

Όπου f η συχνότητα του περιοδικού φαινομένου, Η το χαρακτηριστικό μήκος του σώματος (στην περίπτωση του κτιρίου λαμβάνεται το ύψος) και U_∞ η αδιατάραχτη ταχύτητα.

ΜΕΘΟΔΟΛΟΓΙΑ

Ορισμός πεδίου

Σύμφωνα με το θεμελιώδες θεώρημα διαχωρισμού της διανυσματικής ανάλυσης (Helmholtz), οποιοδήποτε διανυσματικό πεδίο πεπερασμένο, συνεχές και διαφορίσιμο μπορεί να διαχωρισθεί σε ένα αστρόβιλο και ένα στροβιλό τμήμα. Συνεπώς, το πεδίο ταχύτητας μπορεί να εκφρασθεί ως :

$$\mathbf{U}(\mathbf{x},\mathrm{t}) = \mathbf{U}_\infty(\mathbf{x},\mathrm{t}) + \nabla\Phi + \nabla \times \mathbf{A} \qquad 0.2$$

Η ροή αέρα που μελετάται θεωρείται ασυμπίεστη, αφού ο αριθμός Mach ανήκει στο εύρος 0-0.3.

$$\nabla \cdot \mathbf{u} = 0 \qquad 0.3$$

Βάσει της διανυσματικής ιδιότητας $\nabla\times\nabla = 0$ ένα αστρόβιλο πεδίο (γ = 0) εκφράζεται ως:

$$\mathbf{u} = \nabla\Phi \qquad 0.4$$

Ως ιδανική χαρακτηρίζεται η μη συνεκτική, ασυμπίεστη και αστρόβιλη ροή επομένως οι 0.3 , 0.4 οδηγούν στην γραμμική εξίσωση Laplace (Μ.Δ.Ε ελλειπτικού τύπου).

$$\nabla^2\Phi = 0 \qquad 0.5$$

Στην μη συνεκτική (panel) μεθοδολογία που εφαρμόζεται, το αστρόβιλο πεδίο $\nabla\Phi$ αντιστοιχεί στην ιδανική ροή και το στροβιλό $\nabla \times \mathbf{A}$ στον ελεύθερο δυναμικό ομόρρου $\mathrm{S_W}$.

Μέθοδος συνοριακών στοιχείων

Η μη πλεγματική μέθοδος των συνοριακών στοιχείων βασίζεται στην κατανομή στοιχείων (πηγές, δίπολα) αγνώστων εντάσεων (σ,μ) στα ορισμένα σύνορα του προβλήματος. Τα σύνορα $\mathrm{S_b}$, $\mathrm{S_W}$, S_∞ αποτελούν επιφάνειες (3D) ασυνέχειας και διαχωρίζουν το πρόβλημα σε περιοχές (εσωτερική, εξωτερική, αδιατάραχτη). Η γραμμικότητα της εξίσωσης

Laplace καθιστά δυνατή την υπέρθεση στοιχειωδών λύσεων (οι λύσεις φ_p, μ,σ ικανοποιούν την 0.5)

$$\Phi_p = \frac{1}{4\pi}\sum(A_\mu\,\mu + A_\sigma\sigma) \qquad 0.6$$

Στοιχείο	συντελεστής A	ένταση	Εφαρμογή
Πηγή	$-\frac{1}{\lvert\mathbf{r}\rvert}$	$\sigma = \nabla\lVert\Phi\rVert\cdot\mathbf{n}$	σώματα με πάχος
Δίπολο	$-\frac{\mathbf{r}\cdot\mathbf{n}}{\lvert\mathbf{r}\rvert^3}$	$\mu = -\lVert\Phi\rVert$	παραγωγή στροβιλότητας

Table 0.1: στοιχειώδεις λύσεις Laplace

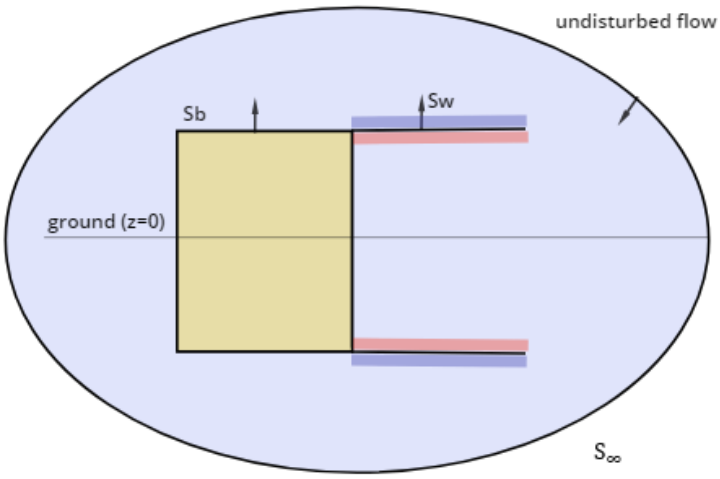

Figure 0.3: Ορισμός πεδίου (2D)

Μοντέλο ομόρρου

Ο ομόρρους αποτελεί την στροβιλή περιοχή (επιφάνεια διάτμησης) που αποβάλλεται από την ακμή εκφυγής του σώματος. Μοντελοποιείται ως συνεχές φύλλο στροβιλότητας δηλαδή ως πλέγμα δινοσωλήνων και η διαχείριση του είναι καθοριστική για την ομαλή εξέλιξη της ροής (μη μόνιμο πρόβλημα). Η επαγόμενη ταχύτητα σε ένα σημείο Α που απέχει απόσταση $\mathbf{r}$ από τον άξονα ενός νήμα στροβιλότητας μήκους $\mathbf{dl}$ και έντασης Γ υπολογίζεται μέσω του νόμου Biot-Savart:

$$\mathbf{u_{ind}} = \frac{\Gamma}{4\pi}\frac{\mathbf{dl}\times\mathbf{r}}{|\mathbf{r}|^3} \qquad 0.7$$

Η ισοδυναμία του παρακάτω σχήματος (6) ,καθιστά εφικτή την μοντελοποίηση του ομόρρου με σταθερές κατανομές διπόλων μ σε κάθε τετράεδρο του πλέγματος δινοσωλήνων.

$$\Gamma_w = -\mu_w = \|\varphi\|_w \qquad 0.8$$

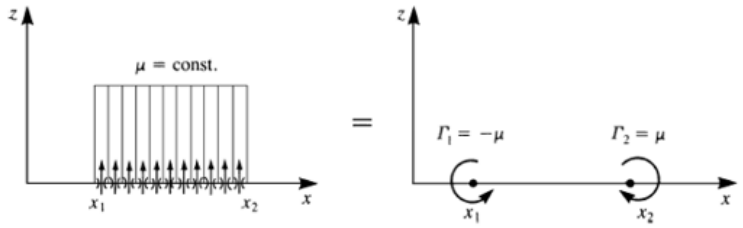

Figure 0.4: Ισοδυναμία μεταξύ σταθερής κατανομής μ κατά μήκος ενός panel και δυο σημειακών στροβίλων στις ακμές του (6).

Επομένως είναι δυνατή η ενσωμάτωση της στροβιλής περιοχής στην έκφραση του δυναμικού και η ταυτότητα του Green (0.6) για τον υπολογισμό του δυναμικού σε ένα σημείο P της επιφάνειας του σώματος S_b λαμβάνει την εξής μορφή :

$$\Phi_p = -\frac{1}{4\pi}\int\left(\frac{1}{|\mathbf{r}|}\sigma + \frac{\mathbf{r}\cdot\mathbf{n}}{|\mathbf{r}|^3}\mu\right) dS_B \; -\frac{1}{4\pi}\int\frac{\mathbf{r}\cdot\mathbf{n}}{|\mathbf{r}|^3}\mu_w \, dS_W \qquad 0.9$$

Στην περίπτωση ασυμπίεστου ρευστού, όπως η εξεταζόμενη, ο όρος σ_w μηδενίζεται καθώς η επιφάνεια του ομόρρου δεν μπορεί να παραλάβει ορθές τάσεις.

Επιπλέον, ισχύει το θεώρημα της υλικής διατήρησης της κυκλοφορίας του Kelvin :

$$\frac{D\Gamma}{Dt} = 0 \quad \leftrightarrow \|\Phi\|_{wi,t} = \|\Phi\|_{wi,t-dt} \qquad 0.10$$

Συνεπώς, ο ομόρρους διαχωρίζεται στον μακρινό, με εντάσεις γνωστές από προηγούμενα βήματα βάσει του θεωρήματος Kelvin και στον κοντινό. Ο υπολογισμός της έντασης $\|\Phi\|_w$ του κοντινού ομόρρου είναι καθοριστικός για την σωστή επίλυση του πεδίου και εξαρτάται, όπως θα αναλυθεί στην συνέχεια, από την δυναμική συνθήκη Kutta:

$$\|p\|_{te} = 0 \quad \leftrightarrow \gamma_{te} = 0 \qquad 0.11$$

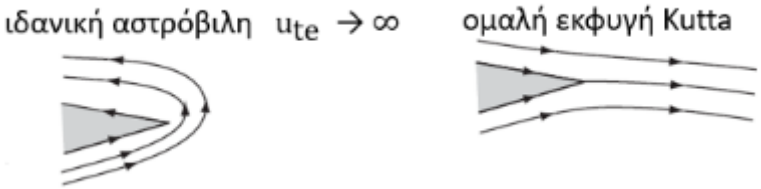

Figure 0.5: Δυναμική συνθήκη Kutta

Όπως φαίνεται στο παραπάνω σχήμα, στην περίπτωση της ιδανικής ροής η ταχύτητα γύρω από πεπερασμένη γωνία τείνει σε πολύ μεγάλες μη ρεαλιστικές τιμές. Η συνθήκη Kutta αποτελεί ένα μαθηματικό ανάλογο της έντονης επίδρασης των συνεκτικών όρων στην ακμή εκφυγής.

Στην πραγματικότητα η ροή αποκολλάται από όλες τις ακμές του ορθογωνικού σώματος. Η αποκόλληση που επιδρά αισθητά στην κατανομή της πίεσης και μοντελοποίειται με τον ελεύθερο δυναμικό ομόρρου στο πλαίσιο της διπλωματικής εργασίας απεικονίζεται στο Figure 0.6.

Περίπτωση αποκόλλησης

Η επιθυμητή τοπολογία του ομόρρου απεικονίζεται στο παρακάτω σχήμα, καθώς και οι δυο διακριτές ζώνες που προκύπτουν από την αποκόλληση της ροής.

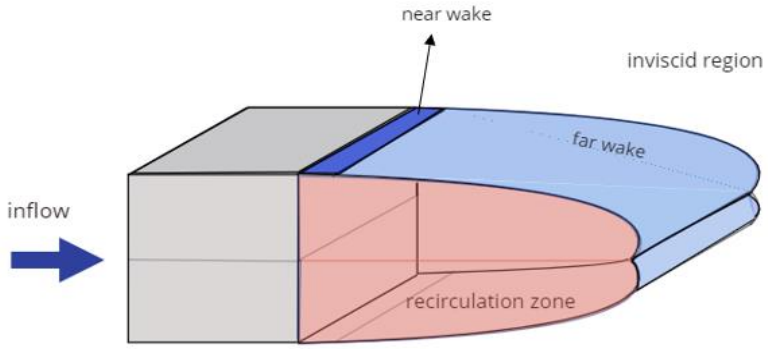

Figure 0.6: Αποκόλληση της ροής και διαχωρισμός του πεδίου σε δύο περιοχές A, B

Το πεδίο πιέσεων συνδέεται με τις ταχύτητες μέσω της εξίσωσης διατήρησης ενέργειας Bernoulli. Στην εξεταζόμενη περίπτωση, κατά την μετάβαση από την μη συνεκτική A στην συνεκτική περιοχή B η μηχανική ενέργεια δεν διατηρείται ($\Delta h \neq 0$) (14).

$$\frac{\partial \varphi_A}{\partial t} + \frac{{U_A}^2}{2} + \frac{P_A}{\rho} = \frac{\partial \varphi_B}{\partial t} + \frac{{U_B}^2}{2} + \frac{P_B}{\rho} + \Delta h \qquad 0.12$$

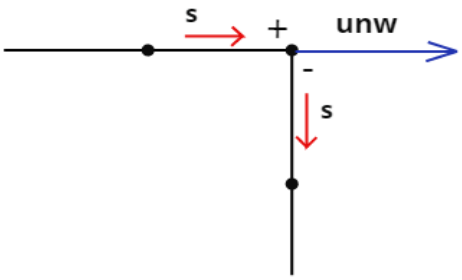

Figure 0.7: Η ροή αδυνατεί να αλλάξει διεύθυνση 90^o και αποκολλάται

$$\mathbf{U}^{-} \cdot \mathbf{s} = 0 \qquad 0.13$$

Η παραπάνω συνθήκη ανακοπής αποτελεί χαρακτηριστικό της αποκόλλησης και εμφανίζεται στην πρώτη σειρά panels κατάντι της ακμής εκφυγής (12)

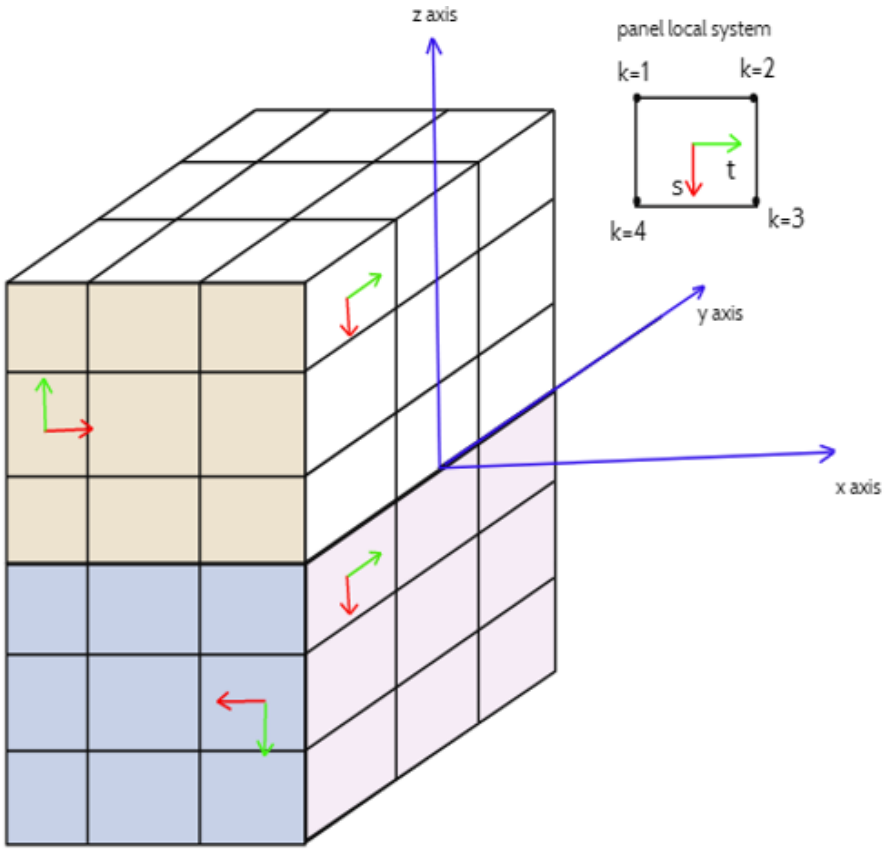

Figure 0.8: Διακριτοποίηση του στερεού σώματος σε τετράπλευρα στοιχεία (panels).

Στο κέντρο ελέγχου κάθε panel επιβάλλεται η συνθήκη μη εισχώρησης :

$$\mathbf{U} \cdot \mathbf{n} = 0 \qquad 0.14$$

Διατύπωση πηγών

Η ιδανική ροή γύρω από το συμμετρικό σώμα κατά την οποία ισχύει $\Gamma_{body} = 0$ μπορεί να επιλυθεί αμελόντας τα δίπολα και συνεπώς η άγνωστη κατανομή είναι αυτή των πηγών σ.

$$\mu = \|\varphi\| = 0 \tag{0.15}$$

$$\Phi_p = -\frac{1}{4\pi}\int \frac{1}{|\mathbf{r}|}\sigma \, dS_B \tag{0.16}$$

Με την επιβολή της συνθήκης μη εισχώρησης σε κάθε panel του σώματος και δεδομένου ότι $\mathbf{U} = \mathbf{U}_\infty + \nabla(-\frac{1}{4\pi}\int \frac{1}{|\mathbf{r}|}\sigma \, dS_B)$ προκύπτει το επιθυμητό πεδίο.

Άμεση διατύπωση (Morino & Kuo)

Η αποκόλληση αποτελεί το βασικό χαρακτηριστικό της εξεταζόμενης γεωμετρίας και δεν μπορεί να αμεληθεί, καθώς επηρεάζει αισθητά την κατανομή της πίεσης όπως θα παρουσιαστεί στα αποτελέσματα που προκύπτουν από την υπολογιστική προσομοίωση. Επομένως, κατανέμονται δίπολα και πηγές στην επιφάνεια του σώματος και δίπολα στον ομόρρου. Για να ορισθεί το αλγεβρικό σύστημα κατάλληλα (εξισώσεις = άγνωστοι) μηδενίζεται το εσωτερικό πρόβλημα (τετριμμένη λύση Laplace $\Phi^- = 0$) και με την επιβολή της συνθήκης μη εισχώρησης η ένταση των πηγών καθορίζεται:

$$\sigma = \frac{\partial \varphi^+}{\partial n} = -\mathbf{U}_\infty \cdot \mathbf{n} = 0 \tag{0.17}$$

$$\mu = -\Phi^+ \tag{0.18}$$

$$\Phi_p = -\frac{1}{4\pi}\int \left(\frac{1}{|\mathbf{r}|}(-\mathbf{U}_\infty \cdot \mathbf{n}) - \frac{\mathbf{r}\cdot\mathbf{n}}{|\mathbf{r}|^3}\Phi\right) dS_B + \frac{1}{4\pi}\int \frac{\mathbf{r}\cdot\mathbf{n}}{|\mathbf{r}|^3}\|\Phi\|_w \, dS_W \tag{0.19}$$

Για τον προσδιορισμό της έντασης $\|\Phi\|_w$ χρησιμοποιούνται δύο εναλλακτικές διατυπώσεις της συνθήκης Kutta (κλασική – βασισμένη στην περίπτωση αποκόλλησης).

Εναλλακτικές διατυπώσεις Kutta

Η κλασική μέθοδος (form1) βασίζεται στον μηδενισμό της στροβιλότητας στην ακμή εκφυγής:

$$\boldsymbol{\gamma} = \nabla\mu \times \mathbf{n} \tag{0.20}$$

$$\gamma_{te} = 0 \rightarrow \|\Phi\|_w = \|\Phi\|_{te} = \Phi^+ - \Phi^- \qquad 0.21$$

Επομένως, η άγνωστη κυκλοφορία στον κοντινό ομόρρου προσδιορίζεται άμεσα από την διαφορά του δυναμικού μεταξύ της πρώτης σειράς panel ανάντι και κατάντι αντίστοιχα της ακμής εκφυγής.

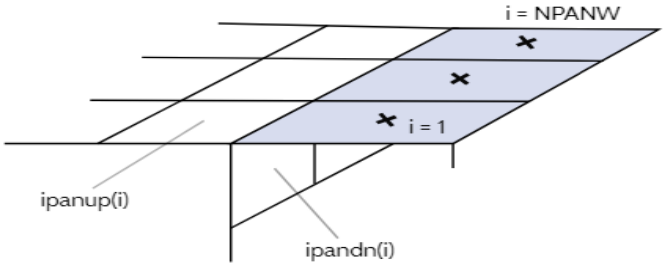

Figure 0.9: Εξάρτηση $\|\Phi\|_w$ από τις εντάσεις του δυναμικού στην περιοχή της ακμής εκφυγής

Η εναλλακτική διατύπωση (form2) που κατασκευάστηκε στο πλαίσιο αυτής της διπλωματικής βασίζεται στα χαρακτηριστικά της αποκόλλησης και όπως θα φανεί παρακάτω οδηγεί σε ένα πιο πεπλεγμένο αριθμητικό σύστημα.

Η εξίσωση Bernoulli εφαρμόζεται στην περιοχή της ακμής εκφυγής και σε συνδυασμό με την συνθήκη Kutta $\|p\|_{te} = 0$ λαμβάνει την παρακάτω μορφή:

$$\frac{\partial \Phi^+}{\partial t} + \frac{U^{+2}}{2} = \frac{\partial \Phi^-}{\partial t} + \frac{U^{-2}}{2} + \Delta h \qquad 0.22$$

όπου τα σύμβολα +,- αντιπροσωπεύουν την πρώτη σειρά panels ανάντι και κατάντι αντίστοιχα της ακμής εκφυγής.

Οι όροι U^2 είναι μη γραμμικοί επομένως για να γραμμικοποιηθεί η εξίσωση, εφόσον το αλγεβρικό σύστημα επίλυσης είναι της μορφής A**X** = B (A μητρώο N×N, X N×1)και εφαρμόζεται η αριθμητική μέθοδος του σταθερού σημείου για την ταχύτητα διαταραχής :

$$\mathbf{u}^2 = \mathbf{u_0} \cdot \mathbf{u} \qquad 0.23$$

Στην πρώτη επανάληψη λαμβάνεται η αρχικοποίηση $u_0 = 0$, ενώ στις επόμενες ${u_0}^i = u^{i-1}$. Η επαναληπτική διαδικασία συγκλίνει όταν

$$\mathbf{u_0} = \mathbf{u} \quad \leftrightarrow \quad \sum_{ndof} (\mathbf{X}^i - \mathbf{X}^{i-1})^2 = 0$$

όπου ndof το πλήθος των βαθμών ελευθερίας (β.ε) του συστήματος **X** και i οι επαναλήψεις σύγκλισης στον ψευδο-χρόνο.

Η διαδικασία γραμμικοποίησης :

$$\mathbf{U}^{+2} = \mathbf{U_s}^{+2} + \mathbf{U_t}^{+2} = \left(\mathbf{U_{\infty s}}^{+} + \mathbf{u_s}^{+}\right)^2 + \left(\mathbf{U_{\infty t}}^{+} + \mathbf{u_t}^{+}\right)^2 =$$

$$= \left(\mathbf{U_{\infty s}}^{+2} + 2\mathbf{U_{\infty s}}^{+}\mathbf{u_s}^{+} + \mathbf{u_s}^{+\,2}\right) + \left(\mathbf{U_{\infty t}}^{+2} + 2\mathbf{U_{\infty t}}^{+}\mathbf{u_t}^{+} + \mathbf{u_t}^{+\,2}\right) =$$

$$= \left(\mathbf{U_{\infty s}}^{+2} + 2\mathbf{U_{\infty s}}^{+}\mathbf{u_s}^{+} + \mathbf{u_{s0}}^{+}\mathbf{u_s}^{+}\right) + \left(\mathbf{U_{\infty t}}^{+2} + 2\mathbf{U_{\infty t}}^{+}\mathbf{u_t}^{+} + \mathbf{u_{t0}}^{+}\mathbf{u_t}^{+}\right) =$$

$$= \mathbf{u_s}^{+}\left(2\mathbf{U_{\infty s}}^{+} + \mathbf{u_{s0}}^{+}\right) + \mathbf{u_t}^{+}\left(2\mathbf{U_{\infty t}}^{+} + \mathbf{u_{t0}}^{+}\right) + \left(\mathbf{U_{\infty s}}^{+2} + \mathbf{U_{\infty t}}^{+2}\right)$$

Δεδομένου ότι η ταχύτητα διαταραχής εκφράζεται ως $u(\Phi_{pi}, \|\Phi\|_{wj}) = \Phi_p(\Phi_{pi}, \|\Phi\|_{wj})$ και λαμβάνοντας υπόψιν ότι το πήδημα ενέργειας Δh είναι άγνωστο, το αλγεβρικό σύστημα δεν είναι κατάλληλα ορισμένο

β.ε: $\Phi_p, \|\Phi\|_w, \Delta h$ (NPANB+2NPANW) < μη εισχώρησης, Bernoulli (NPANB +NPANW)

Επομένως, κρίνεται αναγκαία η ενσωμάτωση μιας ακόμη εξίσωσης η οποία είναι η συνθήκη ανακοπής 0.13 που αποτελεί χαρακτηριστικό της αποκόλλησης.

Διατύπωση	**Kutta**	$\|\Phi\|_w$	**άγνωστοι(ndof)**	**εξισώσεις επίλυσης**
form1	$\gamma_{te} = 0$	$\|\Phi\|_{te}$	NPANB	μη εισχώρησης
form2	$\|p\|_{te} = 0$	άγνωστη	NPANB+2NPANW	μη εισχώρησης Bernoulli (μη γραμμική → επαναληπτική) ανακοπής

Table 0.2: Σύγκριση εναλλακτικών διατυπώσεων

Αριθμητικές Παράμετροι

Η μη μονιμότητα της ροής οφείλεται στο πρότυπο του ελεύθερου ομόρρου, που μοντελοποιείται ως φύλλο στροβιλότητας και η γεωμετρία του καθορίζεται από αριθμητικές παραμέτρους.

Σε κάθε χρονικό βήμα dt, η γεωμετρία του κοντινού ομόρρου είναι ίδια καθώς το μήκος των panels επιλέγεται να είναι της ίδιας τάξης μεγέθους με το μήκος των panels του σώματος στην γειτονιά της ακμής εκφυγής και η ταχύτητα αποβολής $\mathbf{U_{nw}}$ του επιλέγεται ως :

$$dl_w \sim dx \qquad 0.24$$

$$\mathbf{U_{nw}} = \mathbf{U_\infty} \qquad 0.25$$

$$dt = \frac{dl_w}{U_{nw}} \qquad 0.26$$

Ο μακρινός ομόρρους παράγεται με υπολογισμό της επαγόμενης ταχύτητας του πεδίου σε κάθε κόμβο του πλέγματος και με αντίστοιχη μετακίνηση αυτού. Η ανεξάρτητη μετακίνηση κάθε κόμβου αντιτίθεται στην μοντελοποίηση του ομόρρου ως συνεχή επιφάνεια και σε περιπτώσεις έντονης στροβιλότητας (πχ roll up), παρατηρούνται αριθμητικές αστάθειες λόγω της πιθανής στρέβλωσης του πλέγματος.

Όπως έχει αναφερθεί και προηγουμένως μια σταθερή κατανομή διπόλων σε ένα panel ισοδυναμεί με μια κλειστή καμπύλη (τετράπλευρο) που αποτελείται από νήματα στροβιλότητας έντασης $\Gamma_w = \|\Phi\|_w$. Στον άξονα ενός νήματος και σε μια περιοχή ακτίνας ε γύρω από αυτόν η επαγόμενη ταχύτητα λαμβάνει πολύ μεγάλες μη ρεαλιστικές τιμές, γεγονός που εξηγείται από την αμέληση των συνεκτικών όρων. Για αυτόν τον λόγο ενσωματώνεται μια συνάρτηση φίλτρου $J_{E(r)}$, κατά τον υπολογισμό της επαγόμενης ταχύτητας σε ένα σημείο Α που βρίσκεται σε απόσταση r από τον άξονα του νήματος , η οποία προσομοιώνει την συνεκτικότητα στην περιοχή του πυρήνα ε.

$$J_{E(r)} = 1 - e^{-(\frac{r}{\varepsilon})^2} \quad \rightarrow \quad \mathbf{U'} = J_{E(r)}\mathbf{U} \qquad 0.27$$

Η ακτίνα του πυρήνα επιλέγεται ως $\varepsilon \sim dl_w$ καθώς, όπως θα παρουσιαστεί στα αποτελέσματα, το επαγόμενο πεδίο ταχυτήτων είναι ευαίσθητο στην μεταβολή της.

ΑΠΟΤΕΛΕΣΜΑΤΑ

Εφόσον επιλέχθηκε αποβολή ομόρρου μόνο από την πάνω ακμή και όχι από τα πλάγια, τα αποτελέσματα που παρουσιάζονται σε αυτή την ενότητα αφορουν την καμπύλη που απεικονίζεται στον παρακάτω σχήμα.

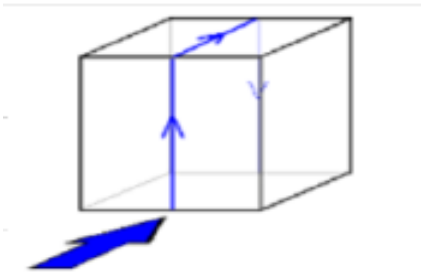

Figure 0.10: y = 0, 2D μοντελοποίηση αποκόλλησης *(13)*

Model1	
D(m) – x άξονας	0.125
H(m) – z άξονας	0.100
B(m) – y άξονας	0.150
$U_\infty x$ (m/s)	4.5

Table 0.3

Ιδανική ροή

Λόγω της ορθογωνικής γεωμετρίας δεν υπάρχει πύκνωση στην οποία συγκλίνει η λύση στις ακμές. Επομένως, επιλέγεται ομοιόμορφο πλέγμα και γίνεται η επίλυση του ισοδύναμου συμμετρικού συστήματος (μείωση υπολογιστικού χρόνου Figure 0.12) μέχρι να σχηματιστεί η ζώνη ανακυκλοφορίας. Οι βαθμοί ελευθερίας μειώνονται στους μισούς NDOF = 1484.

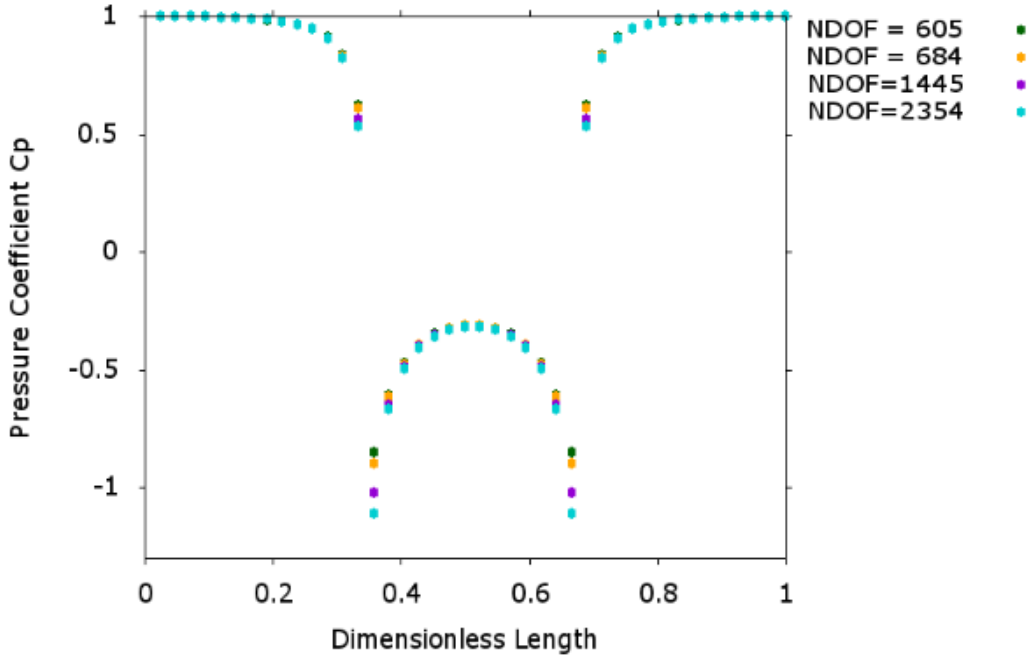

Figure 0.11: Ανάλυση ευαισθησίας πλέγματος

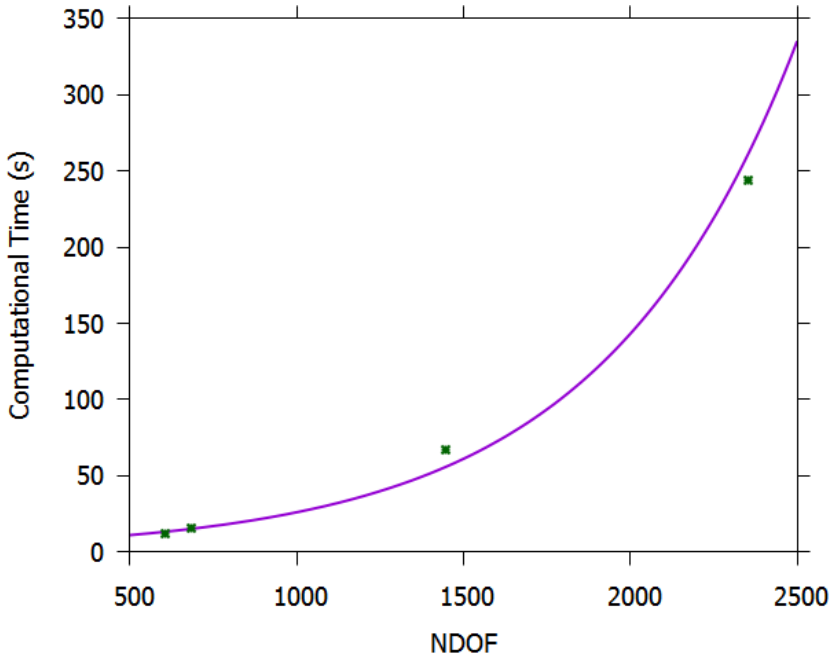

Figure 0.12: εκθετική αύξηση υπολογιστικού χρόνου συναρτήσει βαθμών ελευθερίας

Αποκόλληση – μη μόνιμη ροή

Η εφαρμογή της κλασικής μέθοδου (form1) αποφέρει τα χαρακτηριστικά της αποκόλλησης με την εξέλιξη της ροής.

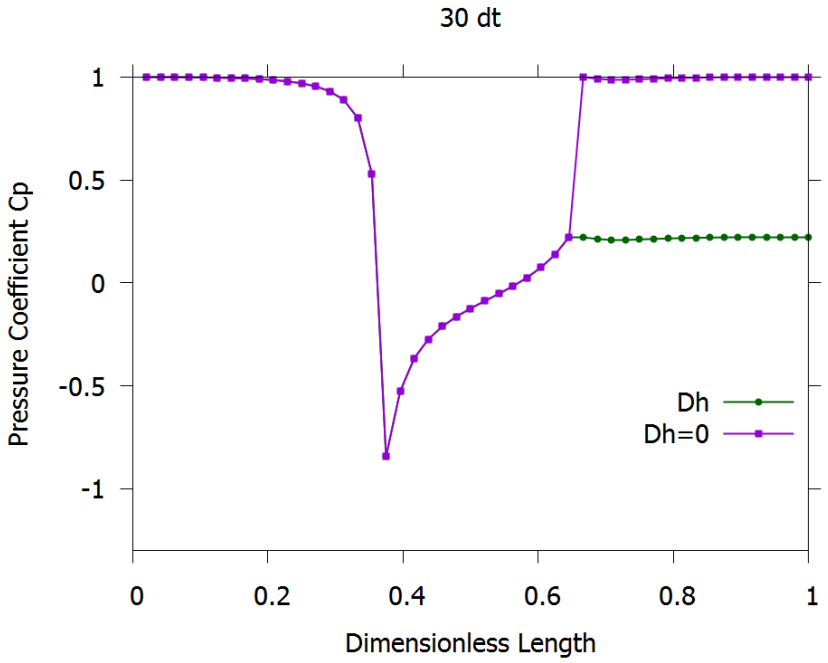

Figure 0.13: Ο όρος Δh (πήδημα ενέργειας) είναι απαραίτητος στην περίπτωση της αποκόλλησης ↔ επαλήθευση συνθήκης Kutta

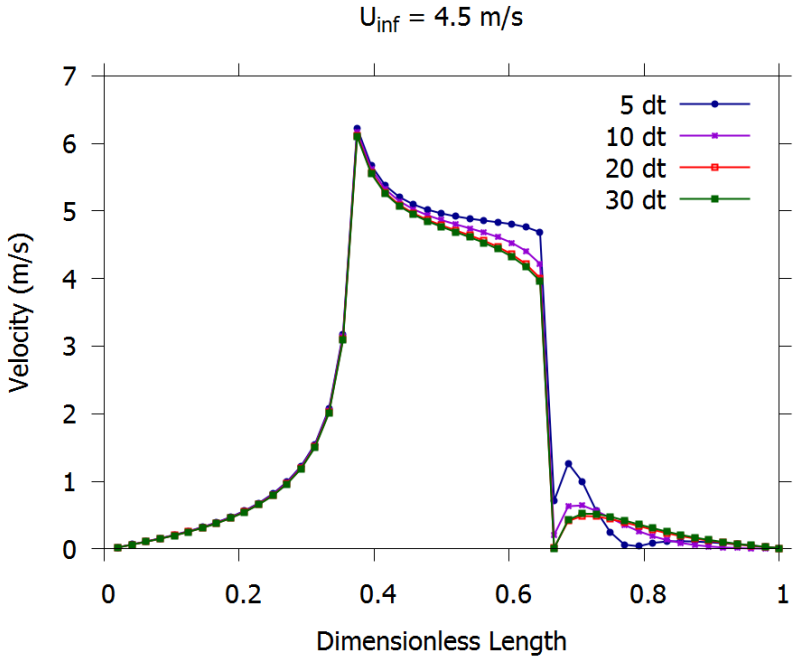

Figure 0.14: Εμφάνιση της αναμενόμενης ανακοπής *(12)* με την εξέλιξη της ροής.

Πεδίο ροής

Τα αποτελέσματα αφορούν επίλυση σε 30 χρονικά βήματα και εφαρμογή της κλασικής μεθοδολογίας. Το προφίλ ταχύτητας συγκρίνεται με την περίπτωση της ιδανικής ροής και με αντίστοιχα αποτελέσματα από CFD (4) προσομοιώσεις.

Παρόλο που η τοπολογία του ομόρρου δεν έχει την επιθυμητή μορφή (σχηματισμός ζώνης ανακυκλοφορίας), η προσομοίωση της αποκόλλησης οδηγεί σε ικανοποιητικά αποοτελέσματα στην περιοχή του κοντινού ομόρρου, όπως φαίνεται στο Figure 0.16.

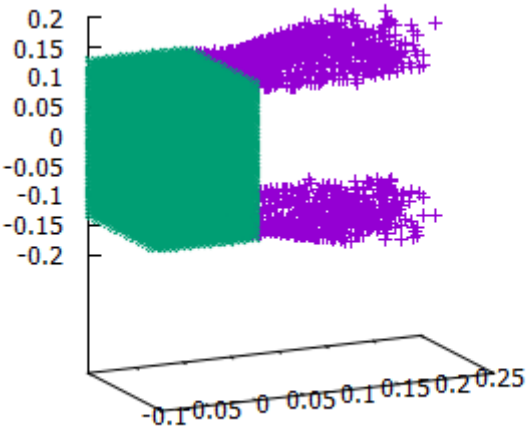

Figure 0.15

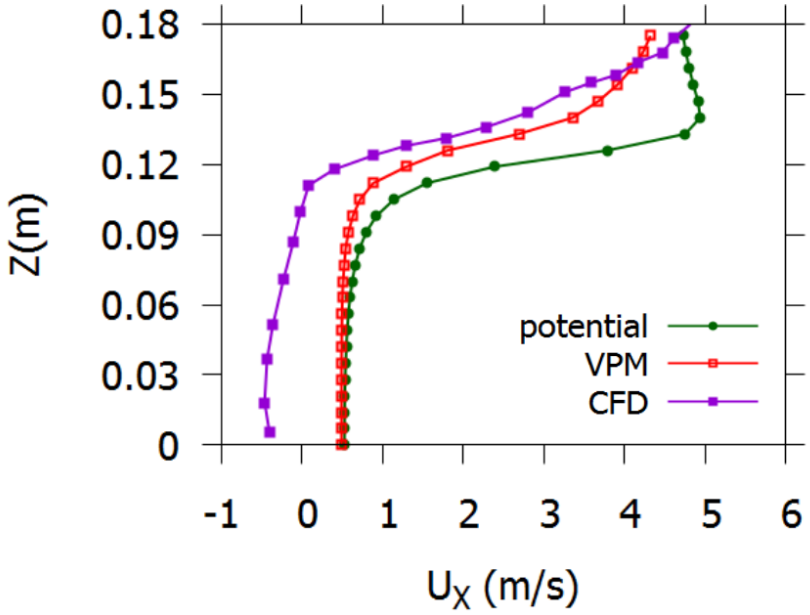

Figure 0.16

Προσομοίωση ΑΟΣ

Στην μη συνεκτική μεθοδολογία που εφαρμόζεται, δεν είναι δυνατόν να προσομοιωθούν τα συνεκτικά και τυρβώδη χαρακτηριστικά που συναντώνται στο ατμοσφαιρικο οριακό στρώμα (ΑΟΣ), αλλά μπορεί να εισαχθεί μια κατανομή ταχύτητας $U_{\infty x}(z)$ ανάλογα με την υπολογιστική και πειραματικη προσομοίωση σύγκρισης.

Το προφίλ ταχύτητας (χαμηλή διάτμηση) προκύπτει από τον λογαριθμικό νόμο με σταθερές κ=0.41, $z_o = 0.05$ mm και u* = 0.19.

$$U_{\infty x}(z) = \frac{u*}{\kappa}\ln\left(\frac{z}{z_o}\right) \qquad 0.28$$

Model2	
D(m) – άξονας x	0.110
H(m) – άξονας z	0.110
B(m) – άξονας y	0.110
U_{nw} (m/s)	3.5

Table 0.4: Ταχύτητα αδιαστατοποίησης U_{nw} και διαστάσεις μοντέλου *(3)*

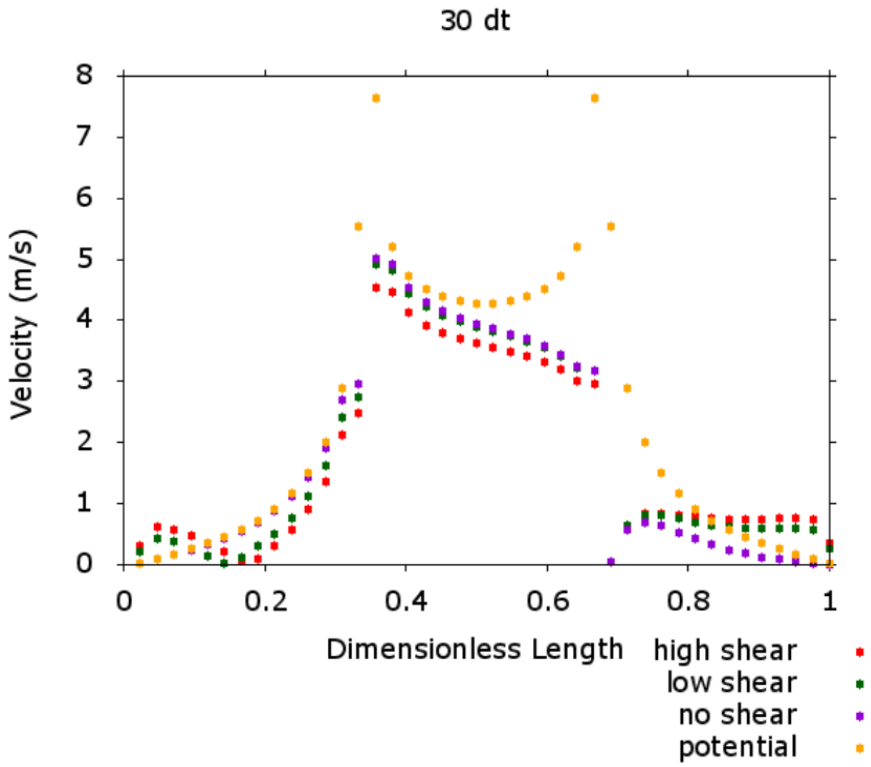

Figure 0.17

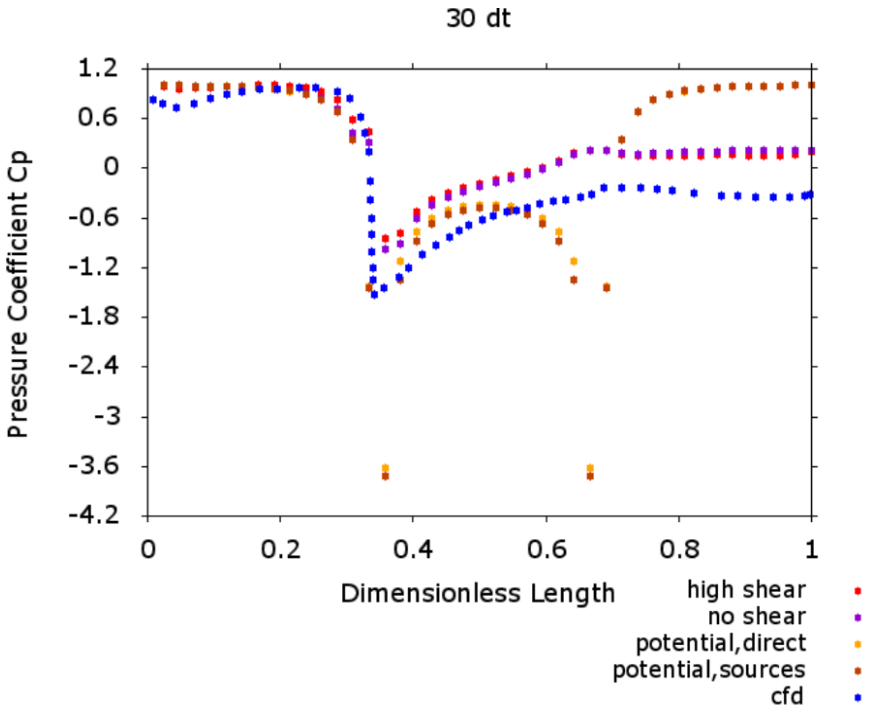

Figure 0.18: Σύγκριση Cp με CFD *(3)*και πειραματικές *(5)* προσομοιώσεις

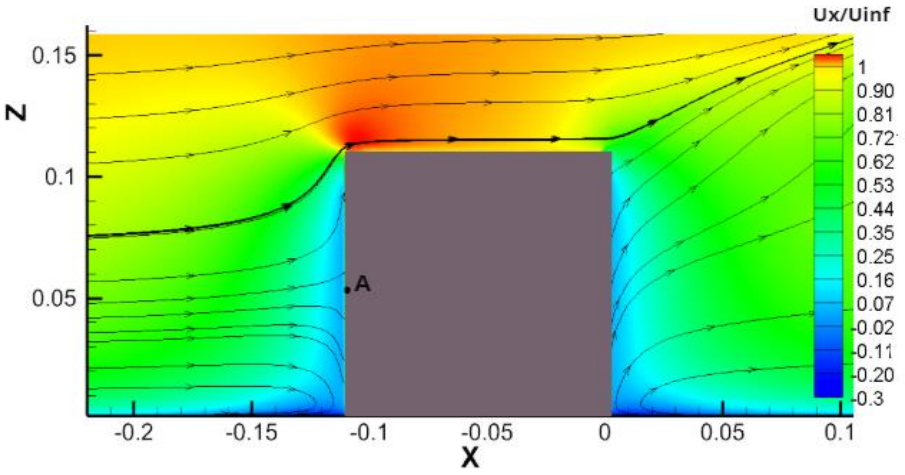

Figure 0.19: Πεδίο ροής και μετατόπιση σημείου ανακοπής A

Η κατανομή της ταχύτητας που χρησιμοποιήθηκε ως είσοδος στον κώδικα, δεν οδηγεί σε σημαντικές διαφορές στο Cp. Παρόλαυτα εμφανίζεται η μετατόπιση του σημείου ανακοπής από το έδαφος στο σημείο A γεγονός που οδηγεί στην δημιουργία στροβίλου ανάντι της μετωπικής επιφάνειας του κτιρίου.

Βελτίωση υπολογισμού ταχύτητας

Από τα αποτελέσματα που έχουν παρουσιασθεί και συγκεκριμένα από την τοπολογία του ομόρρου (δεν εμφανίζεται ανακυκλοφορία) σε συνδυασμό με την ανεπιθύμητη υπερπίεση στην υπήνεμη πλευρά, κρίνεται απαραίτητος ο έλεγχος των αρχικών παραδοχών.Μια από τις παραδοχές που επηρεάζει άμεσα το αποτέλεσμα είναι η υπόθεση των σταθερών κατανομών δυναμικού κατά μήκος των στοιχείων του σώματος. Για το έλεγχο εγκυρότητας της παραδοχής έγινε προσομοίωση της ιδανικής μόνιμης ροής με την διατύπωση των πηγών και πράγματι όπως φαίνεται στο παρακάτω σχήμα υπάρχει μεγάλη απόκλιση μεταξύ των δύο διατυπώσεων.

Επομένως, η παραδοχή των σταθερών κατανομών του δυναμικού (συνθήκη μη εισχώρησης στα κέντρα ελέγχου) κατά μήκος των στοιχείων οδηγεί σε λάθος υπολογισμό της ταχύτητας αν δεν γίνει η κατάλληλη παρεμβολή στους κόμβους Figure 0.17.

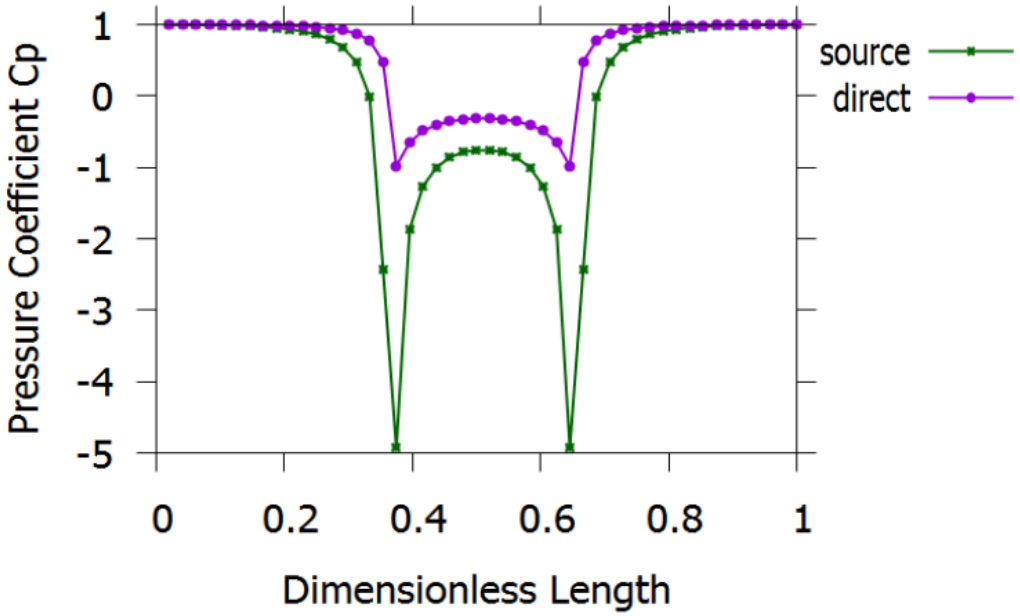

0.29: Ιδανική ροή

ΣΥΜΠΕΡΑΣΜΑΤΑ

Οι πιο σημαντικές παρατηρήσεις από την μέθοδο που αναλύθηκε μετά την εφαρμογή της στην υπολογιστική προσομοίωση του προβλήματος είναι :

- Οι σταθερές κατανομές φ κατά μήκος κάθε panel του σώματος εισάγουν ασυνέχειες στους κόμβους γεγονός που οδηγεί σε λάθος υπολογισμό της ταχύτητας Figure 0.21 .

- Η πίεση στην υπήνεμη πλευρά είναι σχεδόν σταθερή (χαρακτηριστικό αποκολλημένης ζώνης) Figure 0.18

- Η κλασική διατύπωση (form1) οδηγεί στα χαρακτηριστικά της αποκόλλησης Figure 0.14 και σχεδόν στα ίδια αποτελέσματα με την εναλλακτική διατύπωση (form2) η οποία είναι πιο πεπλεγμένη και αργή.

- Μετατόπιση του σημείου ανακοπής στην μετωπική πλευρά με προσομοίωση Α.Ο.Σ Figure 0.19

- Η κατανομή του Cp έχει παρόμοια** μορφή με τα αποτελέσματα της CFD προσομοίωσης. Αισθητή διαφορά στην πίεση με την μοντελοποίηση της αποκόλλησης με τον ελεύθερο δυναμικό ομόρρου (στροβιλή μη συνεκτική μεθοδολογία). Figure 0.18

  ** Η τοπολογία του ομόρρου που προκύπτει δεν είναι η επιθυμητή με αποτέλεσμα να μην δημιουργείται η ζώνη ανακυκλοφορίας (bubble), γεγονός που οδηγεί στην ανεπιθύμητη υπερπίεση (μετατοπισμένο Cp σε σχέση με επιθυμητό).

  Εφόσον η κατανομή του Cp έχει παρόμοια μορφή με την αναμενόμενη προτείνονται δύο περιπτώσεις για μελλοντική διερεύνηση :

- Μοντελοποίηση τμήματος του μακρινού ομόρρου με στοιχεία στροβιλότητας (particles), για την αντιμετώπιση αριθμητικών ασταθειών που πιθανόν προκύπτουν με το συνεχές πλέγμα δινοσωλήνων και οδηγούν σε λάθος υπολογισμό του πεδίου ταχύτητας. Ένα άλλο σημαντικό χαρακτηριστικό των particles είναι η μείωση του υπολογιστικού κόστους, καθώς είναι δυνατή η ομαδοποίηση panels του πλέγματος και η μετατροπή τους σε ένα στοιχείο στροβιλότητας έντασης $\Gamma_w{}^p$.

- Κατάλληλη παρεμβολή του δυναμικού από τα κέντρα ελέγχου του σώματος στους κόμβους. Η συνθήκη ανακοπής (εναλλακτική μέθοδος form2), μπορεί να ενσωματωθεί μέσω του αριθμητικού υπολογισμού της ταχύτητας για να προκύψει η τιμή στον κόμβο κατάντι της ακμής εκφυγής $\Phi^- = \frac{1}{2}(\Phi_{\text{ipdn}} - \Phi_{\text{ipdn+1}})$

  Η επόμενη πρόταση βασίζεται στην αναθεώρηση του ορισμού του πεδίου και συνεπώς σε μια διαφορετική διατύπωση της μεθόδου των συνοριακών στοιχείων προσαρμοσμένη στον διαχωρισμό του πεδίου στις δύο διακριτές ζώνες (συνεκτική – ανακυκλοφορίας)

ΠΡΟΤΕΙΝΟΜΕΝΗ ΔΙΑΤΥΠΩΣΗ

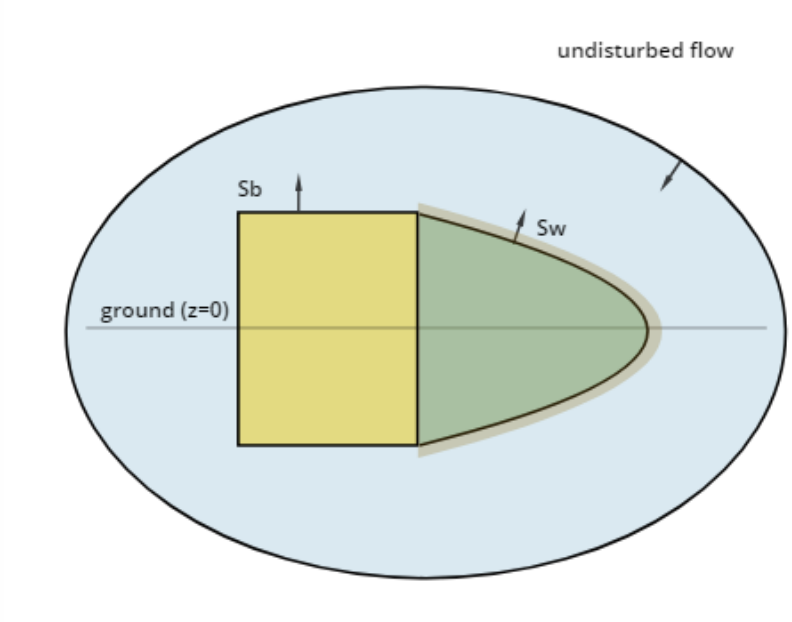

Figure 0.20: Διαφορετικός ορισμός του πεδίου

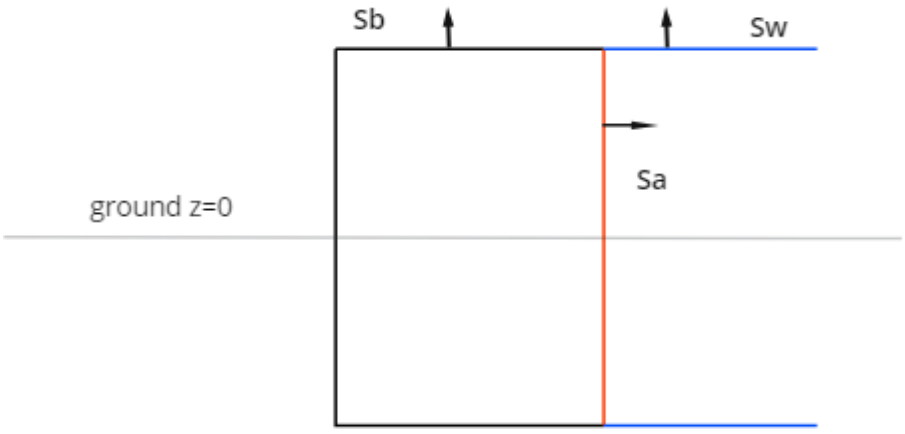

Figure 0.21: σε κάθε επιφάνεια Sa, Sb, Sw κατανέμονται στοιχεία ανάλογα με την φυσική της περιοχής